# Total curvature and total torsion of knotted random polygons in confinement

# Total Curvature and Total Torsion of Knotted Random Polygons in Confinement

**Yuanan Diao[†], Claus Ernst[*], Eric J. Rawdon[♭], and Uta Ziegler[♯]**

[†] Department of Mathematics and Statistics
University of North Carolina Charlotte
Charlotte, NC 28223, USA
[*] Department of Mathematics
Western Kentucky University
Bowling Green, KY 42101, USA
[♭] Department of Mathematics
University of St. Thomas
Saint Paul, MN 55105, USA
[♯] School of Engineering and Applied Sciences
Western Kentucky University
Bowling Green, KY 42101, USA

**Abstract.** Knots in nature are typically confined spatially. The confinement affects the possible configurations, which in turn affects the spectrum of possible knot types as well as the geometry of the configurations within each knot type. The goal of this paper is to determine how confinement, length, and knotting affect the total curvature and total torsion of random polygons. Previously published papers have investigated these effects in the unconstrained case. In particular, we analyze how the total curvature and total torsion are affected by 1) varying the length of polygons within a fixed confinement radius and 2) varying the confinement radius of polygons with a fixed length. We also compare the total curvature and total torsion of groups of knots with similar complexity (measured as crossing number). While some of our results fall in line with what has been observed in the studies of the unconfined random polygons, a few surprising results emerge from our study, showing some properties that are unique due to the effect of knotting in confinement.

## 1. Introduction

In applications involving knot theory to the physical sciences the subjects of the study often call for mathematical models in which random polygons are used as a coarse approximation for physical, rope-like objects that are circular (closed) and have a certain degree of randomness in their formations. Furthermore, biopolymers, such as DNA and RNA, are often subject to spatial confinement with various compactification ratios. In such cases, random polygons in spherical confinement can serve as a coarse model of biopolymers subject to spatial confinement and this is the basis for the study in this article. In [8, 13, 8, 16] we have explored how confinement affects knotting and favors

certain classes of knot types. Confinement also affects the spatial extent of the polygonal configurations, affecting what the configurations look like on average, even within a given knot type. Our goal is to study how confinement affects the total curvature (turning) and total torsion (twisting) in the presence of knotting, and in particular the interplay of these two quantities with confinement, length, and knot complexity.

While there are many different ways to define knot complexity, it is commonly agreed that some knot types are "more complicated" than other knot types. Sometimes a knot type considered complicated by one complexity measure may be considered as simple in terms of a different complexity measure. For example, some knot types with high crossing numbers have small braid indices, and some knot types with small crossing numbers have high braid indices. In this article we concentrate on crossing number as our measure of knot complexity. While there are several competing measures of knot complexity that could be used here, we use the crossing number since it is the most commonly used such measure and none of the alternatives seem to have any intrinsic advantage over the crossing number.

The effects of knot complexity and length on total curvature and total torsion have been studied before for unconfined random knotted polygons for a few simple knot types [28]. In [12] the authors derive an expression for the total curvature of confined equilateral random walks (i.e. confined open chains) that is independent of knotting and compare this result with numerical data obtained from confined equilateral random polygons. The case of the total curvature of confined random polygons (i.e. confined closed chains) is more challenging, in particular because the generation of the confined random polygons is harder than the unconfined case. However, three of the authors of this paper have developed a method for generating confined random polygons efficiently [9, 10, 11]. Furthermore, as has been observed in [8, 14], confined polygons (with a fixed polygon length) form more complex knots than unconfined polygons. This is both bad and good news: Complex knots are more challenging, computationally, to identify, yet complex knots are also rare in unconfined case. The confinement allows us to observe the behavior of complex knots that would not be available in the unconstrained case for the polygon lengths we study.

For these confined polygons we 1) fix the length and vary the confinement radius and 2) fix the confinement radius and vary the length, and observe the effects on total curvature and total torsion. While some of our results fall in line with what has been observed in the studies of the unconfined random polygons, a few surprising results emerge from our study, showing some properties that are unique due to the effect of knotting in confinement. For example, under tight confinement, polygons with a simple knot type (such as the unknot) have an elevated total curvature compared to polygons with more complicated knot types, suggesting that the configurations have had to "self-organize" in some fashion. The counterintuitive fact that knots are less bent than unknots is under certain conditions has also been observed in [5], where the authors study the dependence of knotting probabilities of unconfined semiflexible rings on bending rigidity. Also, the phenomena observed for total torsion are very different

than those for total curvature, and much harder to explain.

This manuscript is organized as follows. In Section 2 we explain how our samples of random polygons are generated, the sample sizes, and how the knot types of the random polygons are determined. Next we explain what is known about total curvature and total torsion for the full set of random polygons, the so-called phantom polygons, in the unconfined case and explore the confined case for phantom polygons. This is followed by Section 4 in which we review what is know about total curvature and total torsion of knotted random polygons in the unconfined case. In Sections 5 and 6 we discuss the effect that knotting complexity has on the total curvature and total torsion of knotted random polygons in the confined case. For each quantity we first present our numerical results and then explain them theoretically. We then discuss the total curvature and total torsion of alternating knots when compared to non-alternating knots and of composite versus prime knots in Section 7. We conclude the article with Section 8 by summarizing the results and indicating open questions of future work.

## 2. Background

In this study, the confined random knots are modeled by equilateral random polygons bounded within a sphere of a given radius. It is important to point out that the definition of the confinement condition affects the distribution of the random polygons. The model adopted for this study is developed by three authors of this paper in [10] and can be described as follows: Consider equilateral random polygons which are "rooted" at the origin (i.e. the polygons have one vertex at the origin) and assume that there is an algorithm that samples such objects with uniform probability. Now consider a confinement sphere $S_R$ of radius $R \geq 1$ with its center at the origin. We keep only the randomly-generated equilateral polygons that are contained in the confinement sphere $S_R$. Note that this algorithm is not based on a direct accept-rejection method (since such a method is extremely inefficient). Instead, the algorithm uses conditional probability density functions that can be explicitly formulated to guide the generation process. Each polygon is generated one edge at a time and there is no rejection involved. Furthermore, this algorithm generates polygons that are totally independent of each other, so no de-correlation is necessary. Since the random polygons are equilateral, the length of the polygon is the same as its number of edges, which we denote as $L$. Note that the same class of equilateral random polygon can be generated directly using an elegant algorithm by Cantarella et al. [2, 4]. Under both approaches, the polygons are rooted at the center of the confinement sphere and thus the smallest confinement radius that can be generated by these algorithms is $R = 1$.

While equilateral random polygons exist in the regime $1/2 \leq R < 1$, there is currently no effective algorithm that can generate such equilateral random polygons. In order to generate polygons for smaller radii, one would have to eliminate the condition that the random polygons are rooted. This is difficult since then one loses the symmetry of the confinement sphere with respect to the starting point. Also note that nobody

knows how rooting affects the statistics of the collected random polygons. One can only speculate that this effect is not significant for the range of data in our study.

The data set used in this paper comes from two sources. A smaller portion of the data ($1,640,000$ polygons) is from one of our earlier papers [8]. In this data set, for each fixed polygon length and confinement radius studied, the sample contains 10,000 random polygons. We refer to this data set as sample 1 in this paper. The larger portion of the data is newer and is aimed at providing a more statistically significant examination of the properties. Two special cases are chosen for this purpose. The first one has a fixed confinement radius at $R = 3$ with polygon lengths ranging from 10 to 90 in increments of 10. The second one has a fixed polygon length of 30 and the confinement radius ranges from 1 to 4.5 with varying increments. For each of these polygon lengths and confinement radii, the sample contains 100,000 random polygons. Overall, this newer data set contains a total of $3,200,000$ random polygons. We refer to this data set as sample 2.

For each of the polygons, we analyze how confinement affects how much the configurations turn (as measured by total curvature) and twist (as measured by the total torsion). For a polygonal knot $K$, its *total curvature* is defined as the sum of the turning angles between its consecutive edges. More precisely, for any three consecutive vertices $X_j$, $X_{j+1}$, and $X_{j+2}$ of $K$, the turning angle between the edges $\overline{X_jX_{j+1}}$ and $\overline{X_{j+1}X_{j+2}}$ is the angle between the vectors $\overrightarrow{X_jX_{j+1}}$ and $\overrightarrow{X_{j+1}X_{j+2}}$, which ranges from 0 to $\pi$. The *total torsion* of $K$ is the sum of all the torsion angles between the oriented planes determined by the consecutive edges. More precisely, for any four consecutive vertices $X_j$, $X_{j+1}$, $X_{j+2}$, and $X_{j+3}$ of $K$, the vectors $\overrightarrow{X_jX_{j+1}}$ and $\overrightarrow{X_{j+1}X_{j+2}}$ determine an oriented plane with normal vector $\overrightarrow{n_1} = \overrightarrow{X_jX_{j+1}} \times \overrightarrow{X_{j+1}X_{j+2}}$, and similarly $\overrightarrow{X_{j+1}X_{j+2}}$ and $\overrightarrow{X_{j+2}X_{j+3}}$ determine a second oriented plane with normal vector $\overrightarrow{n_2} = \overrightarrow{X_{j+1}X_{j+2}} \times \overrightarrow{X_{j+2}X_{j+3}}$. The torsion angle due to these three consecutive edges is defined as the angle between the two normal vectors $\overrightarrow{n_1}$ and $\overrightarrow{n_2}$, which also ranges from 0 to $\pi$.

In the following sections, we analyze the total curvature and total torsion of confined polygons. For each quantity, we summarize the effect of polygonal length $L$ and the confinement radius $R$ on the average values of these geometric quantities. We then study the effect of knotting on these quantities.

A computationally challenging task of this study is to identify the knot types of the random polygons generated. The main methods used for this purpose are the HOMFLYPT polynomial [18] and the `knotfind` algorithm that is part of the `knotscape` package [22]. Sometimes several methods are combined to identify the knot type of a given polygon. For a detailed description of the procedure used see [8, 16].

We concentrate on knot types with up to 10 crossings. While our sample contains much more complicated knots, the number of knots with a fixed crossing number greater than 10 is relatively small and we judge the data for knots above 10 crossings as being no longer robust enough to draw conclusions.

## 3. Total curvature and total torsion for phantom polygons

In this section we analyze the average total curvature and total torsion for phantom polygons with and without confinement.

We refer to the average of a geometric value over all polygons with a given length $L$ and a given confinement radius $R$ as the value of the *phantom polygons*. Thus, in sample 1 each data point for the phantom polygons is the average of $10,000$ random polygons and in sample 2 each data point for the phantom polygons is the average of $100,000$ random polygons.

As length increases for a given confinement radius, more and more complicated knot types become part of the phantom polygon set. This can be explained using the stick number. In particular, the minimal number of edges required to construct a polygon (possibly non-equilateral) of a knot type $K$ is called the *stick number* of $K$, denoted $st(K)$. The crossing number $cr(K)$ and the stick number $st(K)$ are closely related by the inequality [1, 23, 27]:

$$\frac{1}{2}(7+\sqrt{8cr(K)+1}) \leq st(K) \leq \frac{3}{2}(cr(K)+1)\,.$$

In the above inequality there is no assumption that the polygons are equilateral and it is not clear if the same inequality still holds for equilateral polygons. However the lower bound is still valid and this shows that with increasing length, higher crossing number knot types become part of the phantom polygon set. We note that upper bounds on the equilateral stick number can be found in [31] and that the equilateral stick number is the minimal length of the equilateral polygon to form a given knot.

### *3.1. Total curvature and total torsion for unconfined phantom polygons*

For random walks with $L$ bending vertices, which are open polygons with $L+1$ edges and $L+2$ total vertices, the average total curvature is $\pi L/2$ and the average total torsion is also $\pi L/2$ since there is, on average, $\pi/2$ of turning and twisting at each bending vertex. For random polygons with $L$ bending vertices, which are closed polygons with $L$ edges and $L$ total vertices, one would expect the closure condition to affect the expected total curvature in some way. The paper [28] observed that closed unconfined phantom polygons require more total curvature than open chains with the same number of bending vertices, and that amount turns out to be roughly constant for polygons with $L \geq 50$‡. Grosberg [21] later showed that this constant is $3\pi/8$ in the unconfined case. Also, it was observed in [28], and later derived in [21], that closed unconfined phantom polygons require a slightly smaller amount of total torsion than open chains with the same number of bending vertices, which again turns out to be the constant $3\pi/8$ for $L \geq 50$.

In this paper we think of both the total curvature, $C(R,L)$, and total torsion, $T(R,L)$, as functions of the polygon length $L$ and the confinement radius $R$. In the

‡ It is possible that the behavior is different at low numbers of edges.

unconfined case, we set $R = \infty$. With these naming conventions, Grosberg showed [21]:

$$C(\infty, L) = \frac{\pi}{2}L + \frac{3\pi}{8} + O\left(\frac{1}{L}\right) \tag{1}$$

and

$$T(\infty, L) = \frac{\pi}{2}L - \frac{3\pi}{8} + O\left(\frac{1}{L}\right). \tag{2}$$

In addition, in [4] the expected total curvature of unconfined equilateral polygons of length $L$ is given explicitly by an integral. While this integral is not evaluated, the authors give a table of numeric approximations of the expected total curvatures of equilateral polygons for a variety of different lengths $L \leq 64$.

In particular, note that the closure condition adds to the average total curvature and subtracts from the average total torsion relative to open polygons. We see this behavior reappear throughout the remainder of this manuscript.

### *3.2. Total curvature and total torsion for confined phantom polygons*

Since the confinement condition forces random polygons to make sharper and more frequent turns on average, it is quite intuitive that confined random polygons have expected total curvature values larger than their unconfined counterparts. In the extreme case, where the confinement sphere has a diameter close to the unit edge length and the random polygon has to make a nearly 180 degree turn at each step, its average total curvature is close to $\pi L$. On the other hand, if the confinement radius is very large relative to the polygon length, then the polygon behaves like it is unconfined. These two simple cases demonstrate that an extreme confinement condition can almost double the expected total curvature of a random polygon.

One also expects confinement to change the slope of the linear total torsion function. However, instead of increasing the slope of the total torsion function, we would expect confinement to decrease that slope. Indeed, our numerical study shows that a confined random polygon has an expected total torsion smaller than that of its unconfined counterpart.

The total torsion situation is less intuitive and in the following we offer a possible explanation: Envision three consecutive edges $e$, $f$, and $g$ that are coplanar in a plane $P$. Furthermore envision that the three edges are contained in a circle of radius slightly bigger than $1/2$. In Figure 1 we look down at the plane $P$ that contains the three edges and we see the circle of the intersection with the confinement sphere. The edges $e$ and $f$ are marked as solid line segments, while $g$ is shown as a dashed segment in two different positions, with one of its endpoints on the circular arc $ABC$ so that $g$ is unit length. If this endpoint is on the arc $AB$ then the edges $e$, $f$, and $g$ form a torsion angle of $\pi$ and if this endpoint is on the arc $BC$ then $e$, $f$, and $g$ form a torsion angle of 0. It is easy to see that if $e$ and $f$ are as shown in Figure 1 then the arc $BC$ is longer than the arc $AB$, and thus the torsion angle of zero is more likely than the torsion angle $\pi$. Hence, if all positions of the edge $g$ are equally likely then the average torsion angle is less than $\pi/2$.

If we now consider all possible positions of $e$ and $f$ in the plane $P$ and consider where the third line segment could be, then we see that there are often situations like the one shown in Figure 1 where we expect the average torsion angle to be less than $\pi/2$. In a sphere of tight confinement (e.g. $R \approx 0.5$) the situation is not that different from the planar case, since the confinement forces all three edges to be close to a single plane $P$. Thus a small torsion angle is more likely than a large torsion angle.

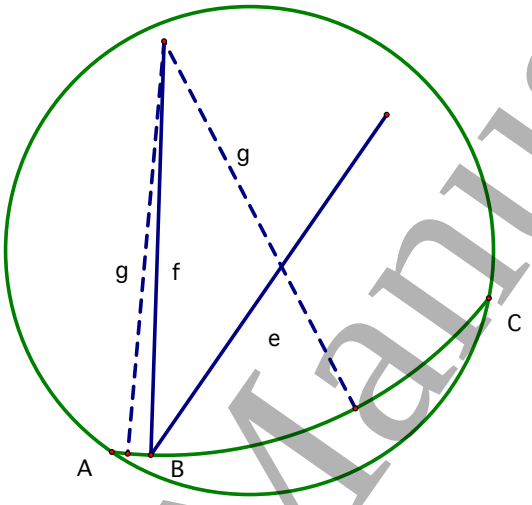


Figure 1: Shown is the plane $P$ containing three consecutive edges $e$, $f$, and $g$ in a sphere of tight confinement. Depending on the choice of the third edge $g$ relative to the point $B$, the torsion angle of the three edges is either 0 or $\pi$.

In fact, numerical observations based on long confined random walks led some of the authors to the following conjecture [12]: As $L \to \infty$ and $R \to 1/2$, the average torsion (per edge) of a random polygon in confinement approaches $\pi/3$.

For confined random polygons we need to modify equations (1) and (2). Figure 2 shows that the total curvature and total torsion of confined phantom polygons grow approximately linearly with increasing length. However, the slope of the lines is no longer $\pi/2$.

We propose an increase to $\frac{\pi}{2} + a(R)$ for total curvature and a decrease to $\frac{\pi}{2} - b(R)$ for total torsion. More specifically, $a(R)$ and $b(R)$ are decreasing positive continuous functions of the confinement radius $R$ satisfying the boundary conditions $a(1/2) = \pi/2$, $\lim_{R \to L/2} a(R) = 0$, $b(1/2) = \pi/6$, and $\lim_{R \to L/2} b(R) = 0$.

The $\frac{3\pi}{8}$ in equations (1) and (2) in the unconfined cases arises as a penalty related to closing a random polygon when compared to a random walk. We propose that the $\frac{3\pi}{8}$ penalty for curvature and torsion is reduced for confined polygons. Without confinement, the expected distance between the endpoints of a random walk of length $L$ is of order $\sqrt{L}$. With confinement, there is a natural bound on the distance between any two points on a open or closed chain. Thus, when $L >> R$, the confinement keeps the endpoints much closer than the unconstrained case, and we would expect less of

a penalty for closure. When $L < 2R$, the polygon is unconfined and the full penalty applies. Thus, we propose to modify $\frac{3\pi}{8}$ by a multiplicative factor $g(R, L)$ that depends on both $R$ and $L$ and which satisfies the boundary conditions $\lim_{R\to 1/2} g(R, L) = 0$ and $\lim_{R\to L/2} g(R, L) = 1$. Note that we propose a common $g(R, L)$ function for both $C(R, L)$ and $T(R, L)$.

As in equations (1) and (2) we propose that there is an error term of order $O(1/L)$. In summary we conjecture that there exist functions $C(R, L)$ and $T(R, L)$ (supported by continuous functions $a(R)$, $b(R)$, and $g(R, L)$) given by:

$$C(R, L) = \left(\frac{\pi}{2} + a(R)\right) L + \frac{3\pi}{8} g(R, L) + O\left(\frac{1}{L}\right) \tag{3}$$

and

$$T(R, L) = \left(\frac{\pi}{2} - b(R)\right) L - \frac{3\pi}{8} g(R, L) + O\left(\frac{1}{L}\right). \tag{4}$$

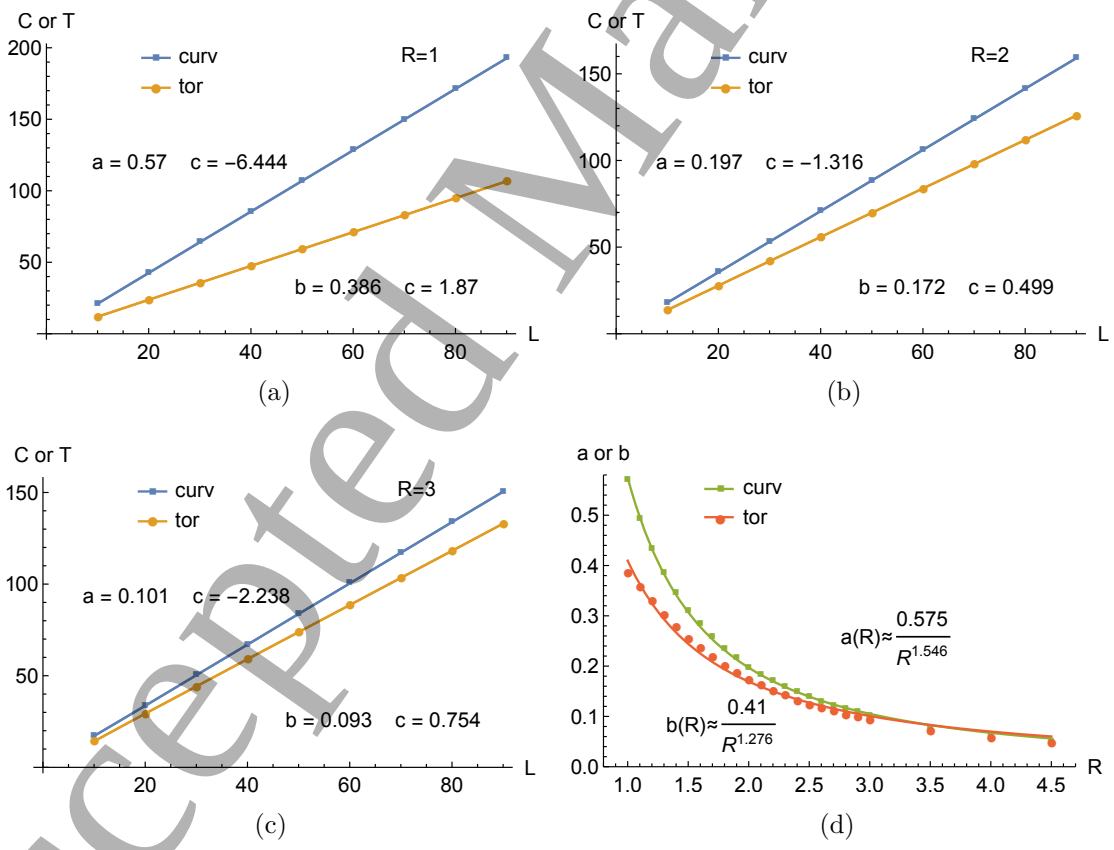


Figure 2: Total curvature and total torsion of the phantom polygons for (a) $R = 1$, (b) $R = 2$, and (c) $R = 3$ together with functions of type $(\pi/2 + a(R))L + \frac{3\pi}{8} g(R, L) + c/x$ (for total curvature) and $(\pi/2 - b(R))L - \frac{3\pi}{8} g(R, L) + c/x$ (for total torsion). The horizontal axis is the polygon length and the vertical axis is the average total curvature or torsion. Part (d) shows the data plots for the functions $a(R)$ and $b(R)$ together with two best fit functions for confinement radii ranging from $R = 1$ to $R = 4.5$.

There are many possible choices for the function $g(R, L)$. In the absence of a theory that would allow us to derive an equation for $g(R, L)$, we choose to construct $g(R, L)$ as simply as possible while satisfying the boundary conditions. Thus in our fitting we use:

$$g(R, L) = \frac{2R - 1}{L - 1} \text{ for } 1/2 \leq R \leq L/2 \text{ and } 1 < L/2 \leq R\,. \quad (5)$$

Moreover, we conjecture that for moderate confinement, e.g. $R \geq 3$, we have $a(R) \approx b(R)$. Figures 2(a-c) are examples of three different radii with the values of $a(R)$ and $b(R)$ shown in the figures. The data for the cases $R = 1$ and $R = 2$ are from sample 1 and the data for the case $R = 3$ is from sample 2. All $R$-squared values of fitting the total curvature and the total torsion of the six cases in Figure 2 are greater than 0.999.

Figure 2(d) contains the data values for the two functions $a(R)$ and $b(R)$ obtained from our data together with fit functions of the form $y = \frac{c}{R^d}$. We note that this type of fit function has been chosen for simplicity. While it provides a good fit for the range of the $R$ values in our study, it does not satisfy the desired boundary conditions.

## 4. The effect of knotting complexity on total curvature and total torsion in the unconfined case

Here we discuss what is known about the total curvature and total torsion of unconfined random polygons that are knotted, coming from the paper [28]. The effect on the total curvature and the total torsion by knot complexity is quite small compared to the total curvature and total torsion values. One way to better observe this effect is to normalize the functions $C(R, L)$ and $T(R, L)$ from (3) and (4) by subtracting the linear growth term $\pi L/2$ from them, so that the resulting functions (denoted by $C'(\infty, L)$ and $T'(\infty, L)$ respectively) behave roughly as constants $\frac{3\pi}{8}$ or $-\frac{3\pi}{8}$ for phantom polygons. Indeed the data collected at length values between 50 and 500 edges in [28] shows that the phantom polygons line up as expected at the constants $\frac{3\pi}{8}$ or $-\frac{3\pi}{8}$, respectively.

Next, in [28] the authors looked at random polygons with a fixed knot type. Since nontrivial knots have a lower probability of occurring without confinement than with confinement, only knot types with at most six crossings were analyzed. For a fixed knot type $K$ we will denote the normalized functions for curvature and torsion by $C'_K(\infty, L)$ and $T'_K(\infty, L)$, respectively. It was reported that $C'_K(\infty, L)$ decreases linearly and $T'_K(\infty, L)$ increases linearly with length $L$.

In the case of the unknot, $C'_{0_1}(\infty, L)$ was entirely below the value of $\frac{3\pi}{8}$ while $T'_{0_1}(\infty, L)$ was entirely above the value of $-\frac{3\pi}{8}$.

For each nontrivial knot type $K$, the function $C'_K(\infty, L)$ crosses the phantom polygon value (namely the constant $\frac{3\pi}{8}$) exactly once. This crossing point is called the *equilibrium length* (for $R = \infty$ relative to total curvature) since the total curvature of phantom polygons and polygons of knot type $K$.

The average of a given quantity (e.g. total curvature) at a given $(R, L)$ pair over the phantom polygons is the baseline behavior of polygons in that setting. For a given

knot type $K$, at an equilibrium $(R, L)$ pair for a given quantity (e.g. total curvature), polygons of knot type $K$ are indistinguishable from the the phantom polygons relative to that quantity. In other words, at an equilibrium, the configurations of knot type $K$ are indistinguishable from the baseline relative to the mean of the quantity. At non-equilibrium $(R, L)$ pairs, one can observe whether the average values for polygons of knot type $K$ are elevated or depressed relative to the baseline. As such, the equilibrium values provide landmarks for changes in behavior relative to the baseline. In this paper, for a given knot type $K$, we observe equilibrium lengths when we fix confinement radii and observe equilibrium radii when we fix lengths.

We observe an equilibrium for total torsion as well. In particular, the curve $T'_K(\infty, L)$ crosses the phantom polygon curve exactly once, yielding an equilibrium length relative to total torsion. Note that the unknots do not have equilibrium values in the unconfined case.

These equilibrium lengths in [28] occur for both total curvature and total torsion at length values between 200 and 350 edges, which are much longer than the polygons in our study. However, since confinement increases the probability of complex knotting, we do have more complicated knots at shorter length values. Thus, one would expect this crossover phenomenon to occur at shorter length values for polygons under confinement.

### *4.1. Numerical results, total curvature and total torsion, unconfined:*

To compare these results with our study for confined polygons we need a different normalization than what is used in [28]. We normalize by subtracting $\pi L/2 - \frac{3\pi}{8}$ for total curvature (subtracting $\pi L/2 + \frac{3\pi}{8}$ for total torsion) and then we divide the difference by the length $L$. We call this new normalized quantity $\nabla C_{cr}(\infty, L)$ in the case of curvature and $\nabla T_{cr}(\infty, L)$ in the case of torsion. These values are average differences per vertex. Using the original data from [28] the normalized quantities $\nabla C_{cr}(\infty, L)$ and $\nabla T_{cr}(\infty, L)$ are shown in Figure 3 for some selected crossing numbers.

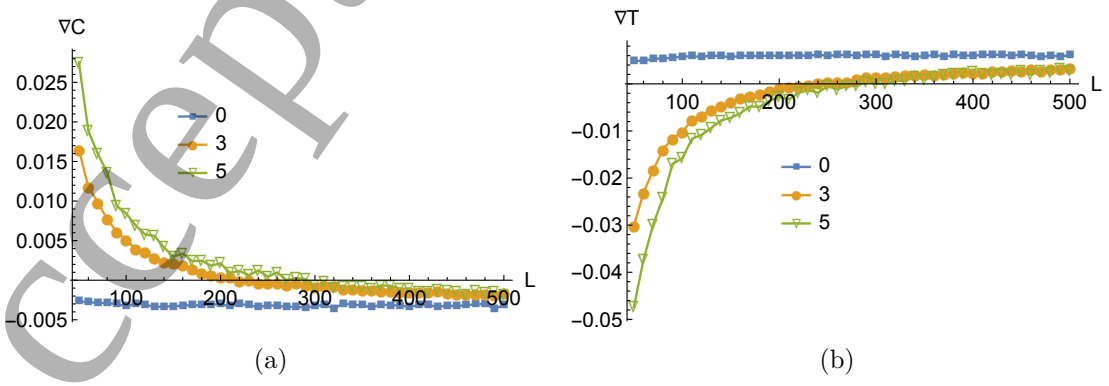


(a) (b)

Figure 3: (a) $\nabla C_0(\infty, L)$, $\nabla C_3(\infty, L)$ and $\nabla C_5(\infty, L)$; (b) $\nabla T_0(\infty, L)$, $\nabla T_3(\infty, L)$ and $\nabla T_5(\infty, L)$.

Using the results in [28] in Figure 3, we make some additional observations:

(i) The graphs of $\nabla C_0(\infty, L)$ and $\nabla T_0(\infty, L)$ are roughly constant. For total curvature the constant is negative and for total torsion the constant is positive.

(ii) For $cr > 0$ the graph of $\nabla C_{cr}(\infty, L)$ is decreasing and concave up. For $cr > 0$ the graph of $\nabla T_{cr}(\infty, L)$ is increasing and concave down.

(iii) There is one equilibrium length for each $cr > 0$ for each of total curvature and total torsion. The point of equilibrium moves to larger $L$ values with increasing knot complexity for both $\nabla C_{cr}(\infty, L)$ and $\nabla T_{cr}(\infty, L)$.

(iv) All graphs approach a horizontal asymptote with increasing $L$.

(v) The functions $\nabla C_{cr}(\infty, L)$ and $\nabla T_{cr}(\infty, L)$ are ordered by crossing number with curves for larger $cr$ having higher $\nabla C_{cr}(\infty, L)$ values and lower $\nabla T_{cr}(\infty, L)$ values.

In the remainder of this article, we see how these behaviors change with differing length and confinement radii. We first concentrate on total curvature, and then later on total torsion.

## 5. The effect of knotting complexity on total curvature in the confined case

In this section, we analyze the effect of knotting complexity on the total curvature of random polygons in confinement. In the first part of this section we show graphs from our collected data and make some observations about the shape of the reported curves. In the second part of this section we introduce a theoretical model that explains the data in the first part.

Similar to [28], which dealt with unconfined polygons, we normalize the curvature of polygons with $cr$-crossing knot types, which we call $C_{cr}(R, L)$. However we can no longer subtract just $\pi L/2 - \frac{3\pi}{8}$ since the confinement radius changes the linear growth rate of total curvature. Here we normalize by subtracting the average values of the phantom polygons at confinement radius $R$ and length $L$ from $C_{cr}(R, L)$ and then we divide the difference by the length $L$. The resulting quantity is again denoted by $\nabla C_{cr}(R, L)$, where $\nabla$ stands for "difference per edge" and $cr$ denotes the (fixed) topological crossing number of the knot types formed by the random polygons. Notice that $\nabla C_{cr}(R, L)$ is bounded by the interval $[-\pi, \pi]$. However, our data shows that the values of $\nabla C_{cr}(R, L)$ are smaller by orders of magnitude when compared to these upper and lower bounds.

### *5.1. Numerical results, total curvature, fixed $R_0$*

In this subsection we present numerical results about the functions $\nabla C_{cr}(R_0, L)$ for fixed $R_0$ values. We concentrate on the case of $R_0 = 3$ using sample 2 data since there are $100,000$ polygons per $(R, L)$-pair and the error margins are smaller. However, on occasion we show data for other lengths and radii from sample 1 with $10,000$ polygons per $(R, L)$-pair to show that the effects hold over a range of lengths and radii.

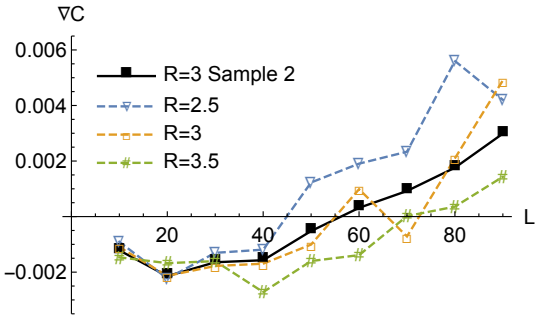


Figure 4: $\nabla C_0(R_0, L)$ for selected values of $R_0$.

*5.1.1. Numerical results, total curvature, fixed $R_0$, unknotted polygons:* Figure 4 shows $\nabla C_0(3, L)$ for the unknot using sample 2 (solid black line) in addition to three dashed curves from sample 1 for radii surrounding $R_0 = 3$. Comparing the two curves of the same radius $R_0 = 3$ provides an indication of how much the error increases when the smaller sample of polygons is used. Note that:

(i) Each curve shows an intersection with the $L$-axis, that is one point of equilibrium with the phantom polygons §. *We note that no such point of equilibrium exists between unknotted random polygons and phantom polygons in the unconfined case.*

(ii) $\nabla C_0(R_0, L)$ is increasing for $L \gtrapprox 20$ and concave up in the range of our data.

(iii) $\nabla C_0(R_0, L)$ does not approach a horizontal asymptote within the range of our data.

(iv) With decreasing radii $R_0$, the curves are shifted up and the point of equilibrium moves to the left.

The equilibrium value for unknots is a significant departure from the unconfined case. We see analogous behavior for nontrivial knots in the next section.

*5.1.2. Numerical results, total curvature, fixed $R_0$, nontrivially knotted polygons separated by crossing number:* Figure 5 shows the numerically obtained curves $\nabla C_{cr}(3, L)$ for $cr \leq 10$. In addition, Figure 6 displays data from sample 1 with dashed lines for the curves $\nabla C_4(R_0, L)$ and $\nabla C_5(R_0, L)$ at $R_0 = 2$, $R_0 = 2.5$, and $R_0 = 3$ alongside data from sample 2 at $R_0 = 3$. The $cr = 4, 5$ are used since there is a sufficient sample of knots to draw the curves arising from sample 1. The graphs show that the curves $\nabla C_{cr}(R_0, L)$ are below the $L$-axis for different values of $R_0$. Note that:

(i) The two curves $\nabla C_{cr}(3, L)$ for $cr = 4$ and $cr = 5$ each have two points of equilibrium with the phantom polygons. *We note that only one such point of equilibrium exists in the unconfined case.* The two points of equilibrium for $cr = 4$ occur at $L \approx 40$ and $L \approx 80$ and for $cr = 5$ at $L \approx 48$ and $L \approx 90$. For the other crossing numbers,

§ The graph contains an intersection with the $L$-axis. But since the length can only be modified in increments of 1, we get $\nabla C_0(R_0, L) \approx 0$ for the equilibrium point. This is true for all equilibrium discussions with a fixed $R_0$.

the evidence for two points of equilibrium is not as convincing. For $cr = 3$ and $cr = 6$, the curve appears to barely fall below the length axis. We do not see the points of equilibrium clearly since the data points are spaced apart by 10 units of length. For $cr \geq 7$, the curves fall below the $L$-axis and one would suspect that they would cross a second time for values of length outside the range of the data. Moreover the distance between the two points of equilibrium tends to get wider with increasing crossing number.

(ii) The values of the curves $\nabla C_{cr}(R_0, L)$ are positive, decreasing, and concave up for short lengths.

(iii) The curves $\nabla C_{cr}(R_0, L)$ do not approach a horizontal asymptote within the range of our study. A horizontal asymptote would seem to be at a value greater than zero.

(iv) For small lengths, the curves are ordered by crossing number with the larger crossing numbers having larger $\nabla C_{cr}(R_0, L)$ values. The ordering of the curves by crossing number is hard to see for the larger length values. The evidence that each curve crosses each other curve at least once is pretty strong. However, it is not clear whether each pair of curves (for $cr > 0$) intersects just once, or possibly twice.

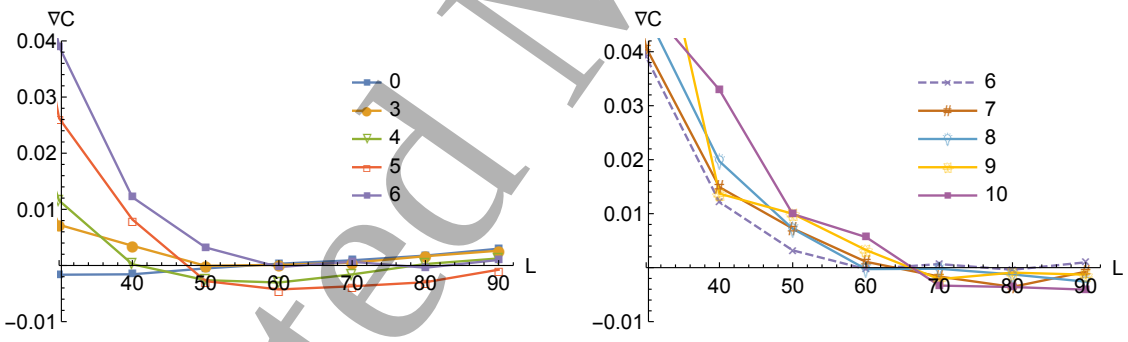


Figure 5: (a) $\nabla C_{cr}(3, L)$ for $cr \leq 6$; (b) $\nabla C_{cr}(3, L)$ for $6 \leq cr \leq 10$.

Figure 6 shows that the observations above are not artifacts of $R_0 = 3$. In particular, we note that:

(i) The equilibrium values shift to the left for lower confinement radii. In other words, more stringent confinement forces equilibria to occur at lower lengths.

(ii) For a fixed crossing number, it appears that lower confinement radii decrease the distance between equilibrium values.

(iii) The curves reverse their order: For small lengths, the larger radii are on top, but for larger lengths, the smaller radii are on top.

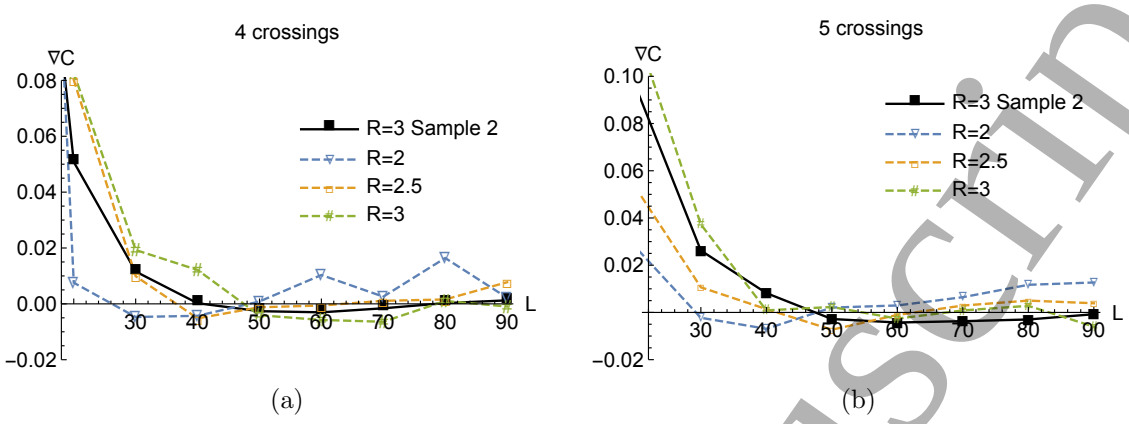


(a) (b)

Figure 6: (a) $\nabla C_4(R_0, L)$ for selected values of $R_0$; (b) $\nabla C_5(R_0, L)$ for selected values of $R_0$.

*5.2. Theoretical model, total curvature, fixed $R_0$:*

In this section, we develop a model for the behavior seen in the data above and conjecture on some behavior that lies beyond the range of the generated data.

Note that when $L < 2R_0$, there is no confinement. As $L$ increases just above $2R_0$, the polygons feel some confinement pressure, but the polygons remain similar in structure to the unconfined configurations described in Section 4. Our goal here is to put a framework around the changes that occur as the confinement pressure continues to increase.

We mention two themes/assumptions that are central to our descriptions throughout the rest of this article. These are intuitive ideas that bear out with our, and other researchers', data.

The first recurring theme/assumption that under at most moderate confinement, complex knotting requires more total curvature, on average, than less complex knotting. For example, consider 12-edge polygons forming 10-crossing knots under no spatial constraints. The minimal number of edges from which the 10-crossing knot types can be formed (known as the *stick number* [19, 29, 31]) is between 10 and 12, depending on the 10-crossing knot type. So at 12 edges, we would expect 10-crossing knot types to have higher total curvature values, on average, than 3-crossing, or even 9-crossing, knot types.

Our second recurring theme is that the highest $\nabla C_{cr}(R_0, L)$ values occur at the smallest $L$ values at which knots with $cr$ crossings can be created. This assumption is an extension, to some extent, of the previous assumption. In particular, we expect the highest crossing knot types possible with $L$ edges to have the highest average total curvature values. So for a given $cr$-value, the greatest difference from the average total curvatures of the phantom polygons should occur at the smallest possible $L$ values. This behavior was observed for unconfined polygons in [28].

With these observations in mind, we next provide a model to describe features of

the $\nabla C_{cr}(R_0, L)$ graphs for unknotted and then nontrivially knotted polygons with a fixed confinement radius $R_0$.

*5.2.1. Theoretical model, total curvature, fixed $R_0$, unknotted polygons:* For $L < 6$, all polygons are unknotted [29] so $\nabla C_0(R_0, L) = 0$. For $L \geq 6$, but close to 6, the average total curvature values of the nontrivial knots are higher than the average for the unknots, and thus we have $\nabla C_0(R_0, L) < 0$ for these $L$ values. As $L$ increases, more and more complicated knots become possible, and these knots increase the average total curvature of the phantom polygons relative to the unknotted polygons, so $\nabla C_0(R_0, L)$ remains negative and decreases. One might expect that $\nabla C_0(R_0, L)$ remains negative, as appears to be the case for unconfined polygons in Figure 3. However, for a long polygon in confinement to be unknotted, it seems to require some "ordering" of the edges in the confinement sphere that actually causes an increase in the average total curvature relative to the phantom polygons. We call this region the *ordered regime*. *Thus, for long lengths $L$, we have $\nabla C_0(R_0, L) > 0$ and there exists an equilibrium length $L_e$, where $\nabla C_0(R_0, L_e) \approx 0$.*

This ordering is a rare occurrence and, thus, as $L$ becomes large with respect to the confinement radius $R_0$, the unknotted random polygons become very uncommon – in fact we conjecture that they become exponentially rare. This result has been proven in the unconfined case [6] but a proof that works under confinement has remained elusive.

*5.2.2. Theoretical model, total curvature, fixed $R_0$, nontrivially knotted polygons separated by crossing number:* Let us begin with some $cr > 0$. For $L < L_{cr}$, where $L_{cr}$ is the minimal length needed to assemble knots with $cr$ crossings, the value $\nabla C_{cr}(R_0, L)$ is undefined. At $L = L_{cr}$, we have $\nabla C_{cr}(R_0, L_{cr}) > 0$. We call this the *knotted regime*, where the average total curvature difference between the knotted polygons and the phantom polygons is driven by the differences in knotting complexity. In this region, the phantom polygons, on average, contains less complicated knots than the $cr$-crossing knots. As $L$ increases, $\nabla C_{cr}(R_0, L)$ decreases since the percentage of more complicated knots among the phantom polygons increases. Next the values of $\nabla C_{cr}(R_0, L)$ reach a local minimum, which we call the *critical length*. Beyond the critical length, it appears that the creation of the $cr$-crossing knots becomes difficult due to the confinement pressure, and some sort of organization of the edges is necessary, as with the unknots above. This organization increases the average total curvature relative to the average over phantom polygons. We call this region the *ordered regime*, which encompasses all $L$ above the critical length. If the value of $\nabla C_{cr}(R_0, \textit{critical length})$ is negative then there are two length values of equilibrium with $\nabla C_{cr}(R_0, L) \approx 0$. More specifically for each equilibrium value $L$ we have that $\nabla C_{cr}(R_0, L-1)$ and $\nabla C_{cr}(R_0, L)$ have opposite signs.

We call the region between the two equilibria the *depressed regime* since $\nabla C_{cr}(R_0, L) < 0$ in this region. In the behavior described above, the depressed regime contains the critical length and parts of both the knotted and ordered regimes. We

call the region where $\nabla C_{cr}(R_0, L) > 0$ the *elevated regime*. In the behavior described in this section, the elevated regime contains parts of both the knotted and ordered regimes. Figure 7 contains a hypothetical curve $\nabla C_{cr}(R_0, L)$(a) outlining the different regimes on the $L$ axis. We note that it is possible that a curve $\nabla C_{cr}(R_0, L)$ has no depressed regime. We use the same terminology in Sections 5.3 and 5.4 where we study the dependence of $\nabla C_{cr}(R, L_0)$ on the radius $R$ for fixed length $L_0$.

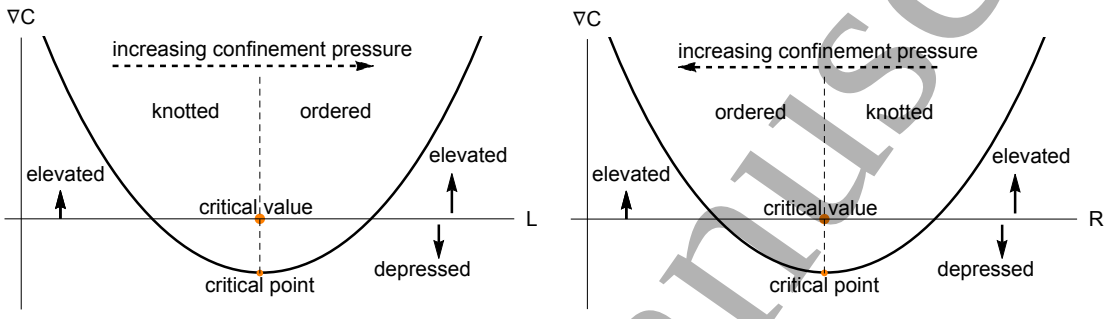


Figure 7: Defining the different regimes for hypothetical (a) $\nabla C_{cr}(R_0, L)$ and (b) $\nabla C_{cr}(R, L_0)$ curves.

An example where there is no depressed regime could be the 6-crossing knots. For the curve $\nabla C_6(R_0, L)$ in Figure 5, it is not clear if the graph falls below the $L$-axis. One of the reasons could be that there are particular knot types where random polygons have a particularly large average total curvature relative to the phantom polygons. Examples of such knot types are composites, see Figure 8. Here $\nabla C_{3_1\#3_1}(R_0, L)$ clearly has no depressed regime and no equilibrium values. Note that by $3_1\#3_1$, we mean both granny and square knots. However, even in this case, we still expect that there is a critical length where $\nabla C_{3_1\#3_1}(R_0, L)$ reaches a minimum. Thus there is still a knotted regime, a critical point, and an ordered regime.

Sketches of typical curves $\nabla C_{cr}(R_0, L)$ for two different radii $R_0$ are shown in Figure 9: For $cr = 0$ in Figure 9(a) and for some values $cr > 0$ in Figure 9(b). In Figure 9(b), the two curves may be interpreted in different ways: For different $R_0$ values and the same $cr$ value or for the same $R_0$ value and different $cr$ values. The curves indicate general shapes – we do not claim that an increased value of $R_0$ leads to exactly the same curve as an increased $cr$ values. As we have described in the previous paragraph it is possible that for some knot types, or even crossing numbers, the curve in Figure 9(b) is shifted up and the critical length is above the $L$-axis.

We summarize our model with the following observations:

(i) For $L < 2R_0$ the polygons are unconfined. The random polygons remain in the knotted regime (the part prior to the critical length). This portion of the graph is consistent with the results from [28].

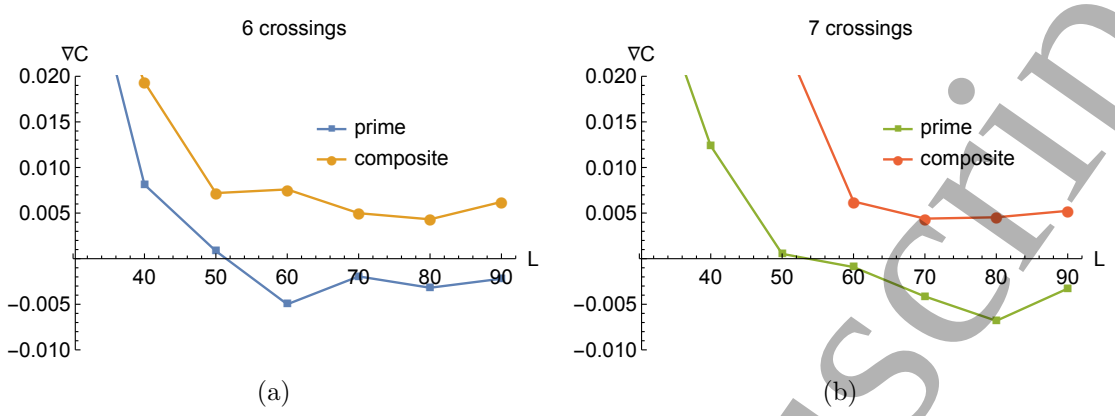


Figure 8: Comparing $\nabla C_{cr}(R_0, L)$ for (a) $cr = 6$ and (b) $cr = 7$ where the knots are separated into prime knot types and composite knot types. The prime knot types have points of equilibrium while the curves for the composite knot types remain entirely above the $L$-axis and have no points of equilibrium.

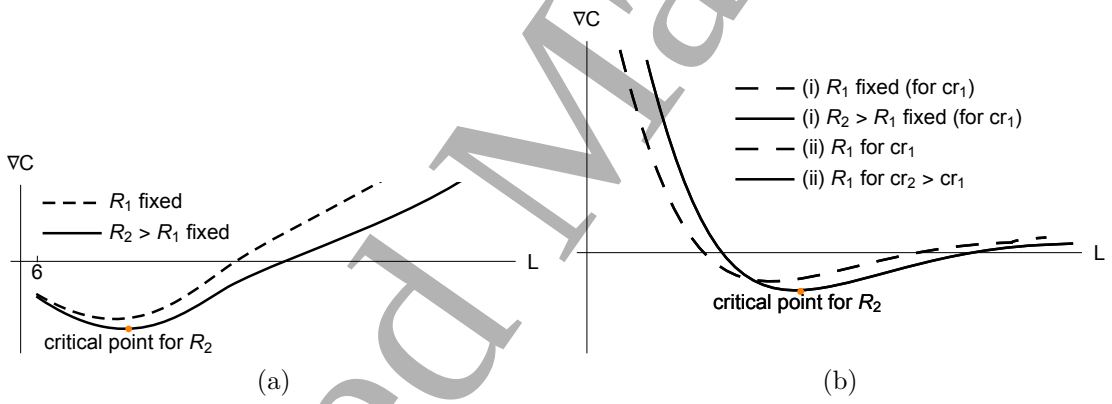


Figure 9: (a) $\nabla C_0(R_0, L)$ for two different values of $R_0$, $R_2 > R_1$; (b) $\nabla C_{cr}(R_0, L)$ for two different values of $R_0$, $R_2 > R_1$, and two crossing numbers, $cr_2 > cr_1$. The two different interpretations of the curves are indicated by (i) and (ii) in the figure legend.

(ii) The unconfined case for unknots (i.e. $cr = 0$) is really a special case where the elevated regime for small lengths is missing, since the unknot can easily be formed at shorter lengths for all radii.

(iii) The above description is based on data for $R \geq 1$. Theoretically, any $R > 1/2$ is possible. As explained earlier, in that situation the curvature of the phantom polygons is nearly $\pi L$. It is unclear what influence knotting complexity plays on $\nabla C_{cr}(1/2 + \epsilon, L)$.

(iv) For $R_0$ fixed, how does the curve change for some $cr_2 > cr_1 > 0$? Our explanation leads to the following: In the elevated knotted regime, larger crossing number knots require relatively more curvature at smaller lengths, and thus the curve for $cr_2$ has higher $\nabla C_{cr}(L, R_0)$ values than the curve for $cr_1$. The critical length and the points

of equilibrium (if they exist) shift to the right for the $cr_2$ curve. The behavior of $\nabla C_{cr_1}(L, R_0)$ relative to $\nabla C_{cr_2}(L, R_0)$ for lengths values beyond the critical length sections of the curves is not clear.

(v) If $R_2 > R_1$ is fixed, then the curve $\nabla C_{cr}(L, R_2)$ has a similar shape to $\nabla C_{cr}(L, R_1)$, but is shifted to the right.

(vi) There is an ordered regime where, with increasing length, the average per-segment total curvature values increase relative to the phantom polygons for polygons of a fixed $cr$. In particular, for a given $cr$ value, there exists an $L_0$ value such that $\nabla C_{cr}(L, R_0) > 0$ for all $L \geq L_0$.

(vii) The critical length is at larger $L$ values for polygons with larger $cr$ values.

### *5.3. Numerical results, total curvature, fixed $L_0$*

In this subsection we present numerical results about the functions $\nabla C_{cr}(R, L_0)$ for fixed $L_0$ values. We concentrate on the case of $L_0 = 30$ using sample 2 data since there are 100,000 polygons per $(R, L)$-pair and the error margins are smaller. However, on occasion we show data for other lengths and radii from sample 1 with 10,000 polygons per $(R, L)$-pair to show that the effects hold over a range of lengths and radii.

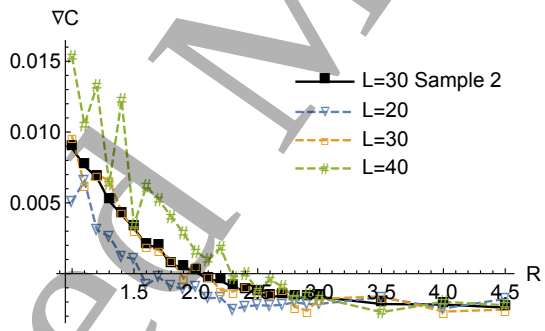


Figure 10: $\nabla C_0(R, L_0)$ for selected values of $L_0$.

*5.3.1. Numerical results, total curvature, fixed $L_0$, unknotted polygons:* Figure 10 shows $\nabla C_0(R, 30)$ for the unknot data using sample 2 (solid black line) in addition to three dashed curves from sample 1 for lengths surrounding $L_0 = 30$. Again, comparing the two curves of the same length $L_0 = 30$ provides an indication of how much the error increases when using the smaller sample of polygons. Note that:

(i) Each curve shows an intersection with the $R$-axis, that is one point of equilibrium with the phantom polygons. *Again, we note that no such point of equilibrium exists between unknotted random polygons and phantom polygons in the unconfined case.*

(ii) $\nabla C_0(R, L_0)$ is decreasing and concave up for all $R$ values.

(iii) $\nabla C_0(R, L_0)$ appears to be approaching a horizontal asymptote as $R \to \infty$.

(iv) With increasing length $L_0$, the curves are shifted up and the point of equilibrium moves to the right.

*5.3.2. Numerical results, total curvature, fixed $L_0$, nontrivially knotted polygons separated by crossing number:* Figure 11 shows the numerically obtained curves $\nabla C_{cr}(R, 30)$ for $cr \leq 10$. The curves $\nabla C_{cr}(R, 30)$ for $cr \leq 6$ are in Figure 11(a) and for $6 \leq cr \leq 10$ are in Figure 11(b). For the latter we only show radii $R \leq 2.5$ because there are few configurations of high complexity for the chosen length at larger radii, which makes the data (if it exists at all) very unreliable. In addition, Figure 12 shows some data from sample 1 similar to Figure 6, but with a restricted range for $R$ to enlarge the area around the $R$-axis. We observe:

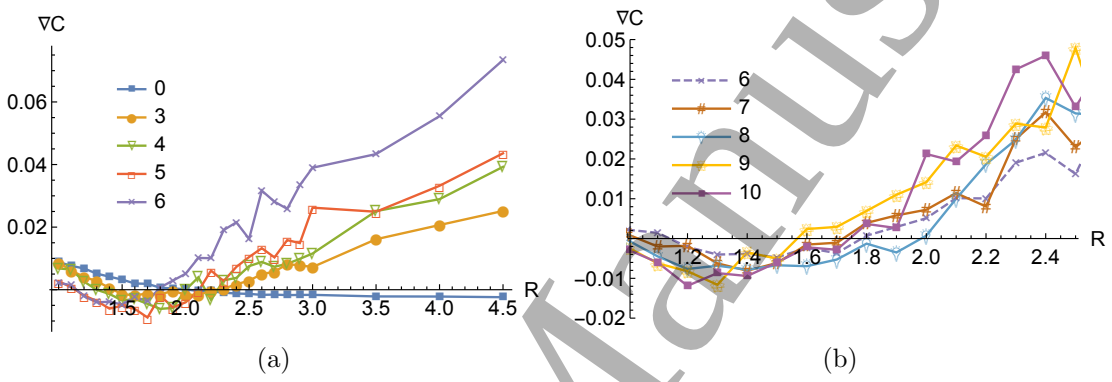


Figure 11: (a) $\nabla C_{cr}(R, 30)$ for $cr \leq 6$; (b) $\nabla C_{cr}(R, 30)$ for $6 \leq cr \leq 10$ and $1 \leq R \leq 2.5$.

(i) Each of the curves $\nabla C_{cr}(R, 30)$ for $3 \leq cr \leq 6$ shows two points of equilibrium with the phantom polygons. In our data the points of equilibrium for the curves $3 \leq cr \leq 6$ occur between $R = 1.3$ and $R = 2.3$. For the crossing numbers $cr > 6$ the evidence for two points of equilibrium is not as convincing. There clearly is one point of equilibrium and one would suspect that there would be another one at some radius $R < 1$ outside the range of our data. Moreover, the distance between the two points of equilibrium tends to get wider with increasing crossing number.

(ii) The values of the curves $\nabla C_{cr}(R, L_0)$ are largest for larger radii. The initial values of $\nabla C_{cr}(R, L_0)$ at $R = 1$ may be negative or positive, depending on the knot complexity of the phantom polygons in comparison with the polygons with crossing number $cr$ at the fixed length $L_0$.

(iii) The graphs do not show evidence of a horizontal asymptote as $R \to \infty$. However, such an asymptote must occur when $R > 2L$, in which case the polygons are unconfined.

(iv) For larger radii, the curves are ordered by crossing number with the larger crossing numbers having larger $\nabla C_{cr}(R, L_0)$ values. Note that the full range of $R$ values is only shown for $cr \leq 6$. Figure 11(b) does not show the larger radii. It appears that at $R = 1$ the curves are ordered by reversed crossing number, with the smaller crossing numbers on top. While the ordering of the curves by crossing number is sometimes hard to see, there is strong evidence that curves for different crossing

numbers intersect each other at least once. In some cases the curves may even cross each other twice.

Figure 12 supports the above conclusion that the two points of equilibrium are not an artifact of the length $L = 30$ since they also show up for other lengths. Note that:

(i) Increasing the length $L_0$ shifts the two points of equilibrium to the right.

(ii) For a fixed crossing number, it appears that increasing lengths result in an increasing distance between the two equilibrium points.

(iii) The curves reverse their order: For small radii $R$ the larger lengths have higher $\nabla C_{cr}(R, L_0)$ values, but for larger radii $R$ the smaller lengths have higher $\nabla C_{cr}(R, L_0)$ values.

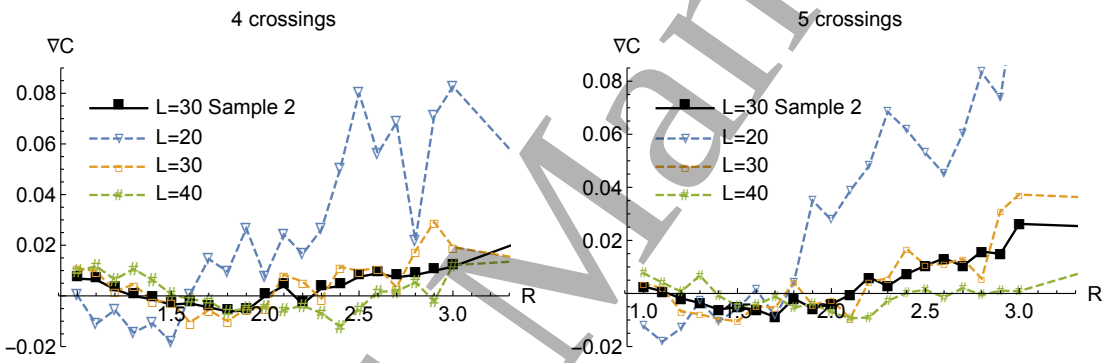


(a) (b)

Figure 12: (a) $\nabla C_4(R, L_0)$ for selected values of $L_0$; (b) $\nabla C_5(R, L_0)$ for selected values of $L_0$.

### *5.4. Theoretical model, total curvature, fixed $L_0$*

In this subsection we introduce a theoretical model for $\nabla C_{cr}(R, L_0)$ where the length $L_0$ is fixed and the radius varies. We stipulate that $L_0$ is long enough so that nontrivial knots with different crossing numbers can be formed.

When considering curves with fixed $L_0$, the following is useful: Decreasing the confinement radius $R$ (using a fixed $L_0$) increases the confinement pressure during the polygon generation in a way that is analogous to using a fixed confinement radius $R_0$ and increasing the length $L$ of the polygons. The fixed $L_0$ case has one significant difference from the fixed $R_0$ case. Namely, for a fixed $L_0$, there is a bound on the maximum complexity of knot types within the set, regardless of the $R_0$. For a fixed $R_0$ and a given knot type, there is an $L$ large enough so that the creation of knots of the given knot type is possible.

For $R > L_0/2$, there is no confinement. For $R$ decreasing below $L_0/2$, confinement occurs and polygons generated under that increasing confinement pressure show a

reduction in the observed unconfined features. As the radius continues to decrease, confinement pressure starts to dominate and the polygons no longer show features of the unconfined model.

When $L = L_0 \geq 6$ is fixed and $cr > 0$ is fixed, up to three different regimes may be encountered, depending on the relationship between the length and the crossing number. We subdivide this situation into three subcases where the crossing number is low, medium, and high relative to $L_0$. For example, the set of unknots, with crossing number 0, lie in the low category for most $L_0$ (except, possibly, when $L_0$ is close to 6). Crossing numbers associated with knot types which can barely be created with $L_0$ edges are in the high category. The medium category lies somewhere in between. For increasing $L_0$ values, the shifts from low to medium and medium to high occur at increasing $cr$ values.

Below we describe the behavior for decreasing $R$ values, i.e. increasing confinement pressure. We begin with the two extreme cases (small and large $cr$ values relative to $L_0$) and then tackle the medium behavior.

*5.4.1. Theoretical model, total curvature, fixed $L_0$, cr is small:* Consider the case where $L_0$ is very large and $cr$ is small, e.g. close to 0. When $R > L_0/2$, the average complexity of the knots is larger than the $cr$-crossing knots, so the average total curvature of the $cr$-crossing knots is smaller than the average for phantom polygons. Thus $\nabla C_{cr}(R, L_0)$ is negative and we are in the depressed knotted regime. As confinement pressure increases ($R$ decreases), the $cr$-crossing knots enter a regime where some ordering of the edges is necessary, which increases the average total curvature to above the average for the phantom polygons. Thus, there is one equilibrium value and no critical value. For small radii $\nabla C_{cr}(R, L_0)$ is positive and we are in the elevated ordered regime.

*5.4.2. Theoretical model, total curvature, fixed $L_0$, cr is high:* In this case, the knot types with $cr$ crossings can barely be constructed (even under confinement) with $L_0$ edges and, thus, have low probability. Knotting contributes to larger average total curvature values than the phantom polygons at all $R$ values. For all radii $\nabla C_{cr}(R, L_0)$ is positive and we are in the elevated knotted regime. There is no point of equilibrium and no critical value. As $R$ decreases below $L_0/2$, the graph decreases due to increasing knot complexity within the phantom polygons.

*5.4.3. Theoretical model, total curvature, fixed $L_0$, cr is medium:* In this case, the $cr$-crossing knots are more complicated than the phantom polygons without confinement. For $R \geq L_0/2$, the values of $\nabla C_{cr}(R, L_0)$ are constant and positive, and we are in the knotted elevated regime. As $R$ decreases, confinement pressure increases the average knot complexity of the phantom polygons and $\nabla C_{cr}(R, L_0)$ decreases. The values of $\nabla C_{cr}(R, L_0)$ decrease (again, recall that we are viewing the graph from right to left) through an equilibrium and obtain a minimum in the depressed regime at a critical

radius. Increasing confinement pressure further causes polygons containing the $cr$-crossing knots to "order" and we move into the ordered regime. Now $\nabla C_{cr}(R, L_0)$ increases and we may obtain a second point of equilibrium. For $R$ values smaller than one, especially very close to 1/2, we have no data and little idea of what occurs.

Sketches of the graphs arising for these three cases are shown in Figure 13. In each image we show curves for two lengths, $L_2 > L_1$. The graphs in Figure 13 must be understood as distinct basic shapes. If one imagines keeping the crossing number fixed and increasing the length $L_0$ then the curves in Figure 13(c) almost continuously change to the shape of Figure 13(b) and from there to the shape Figure 13(a). Thus there could be intermediates where the critical point lies above the $R$-axis or where there is a depressed region as in Figure 13(b) without the second elevated region for small $R$ values.

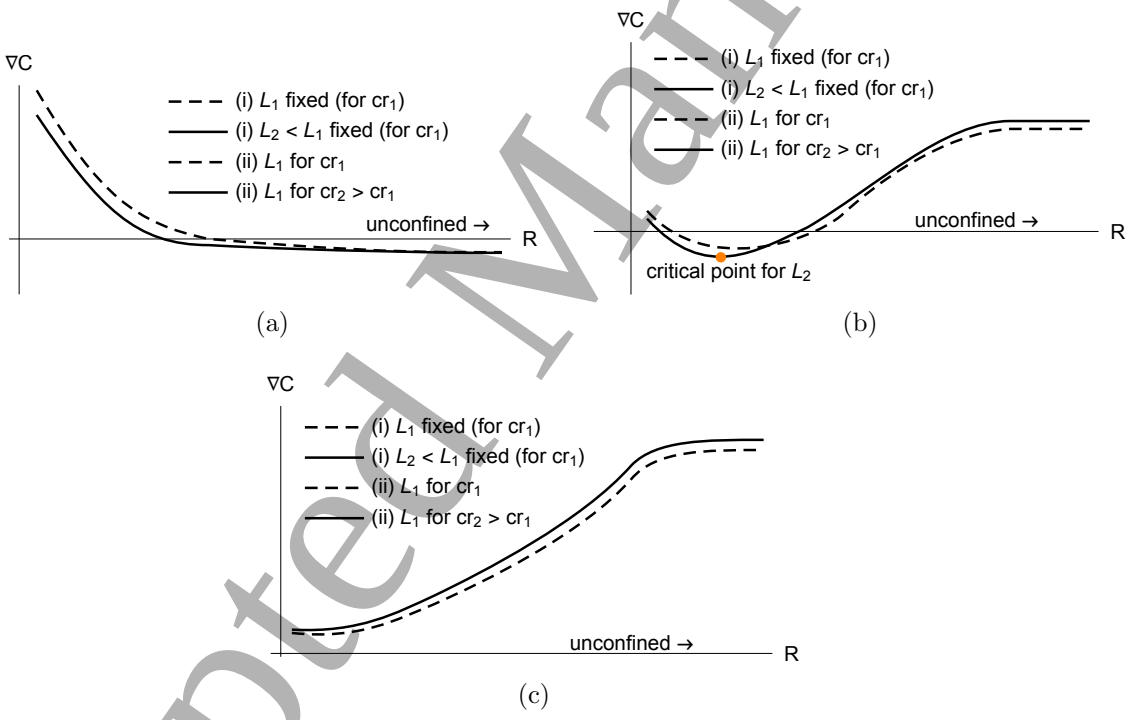


Figure 13: (a) $\nabla C_{cr}(R, L_0)$ for $cr$ small, with $cr_2 > cr_1$, and two different lengths $L_0$, $L_2 > L_1$; (b) $\nabla C_{cr}(R, L_0)$ for $cr$ medium, with $cr_2 > cr_1$, and two different lengths $L_0$, $L_2 > L_1$; (c) $\nabla C_{cr}(R, L_0)$ for $cr$ large, with $cr_2 > cr_1$, and two different lengths $L_0$, $L_2 > L_1$.

We summarize our model with the following observations:

(i) For $R > L_0/2$ the polygons are unconfined. Thus all curves $\nabla C_{cr}(R, L_0)$ end in a horizontal asymptote on the right. For all $cr$ values the random polygons are in the knotted regime, that is the knotting complexity determines the sign of $\nabla C_{cr}(R, L_0)$. For small $cr$ values $\nabla C_{cr}(R, L_0)$ may be negative, and for all other $cr$ values $\nabla C_{cr}(R, L_0)$ is positive.

(ii) For small $R$ values, $\nabla C_{cr}(R, L_0)$ is positive for most of the $cr$ and $L_0$ values in our data set (i.e. we are in the elevated regime). This either happens because we are still in the knotted regime (if $cr$ is large) or we have entered the ordered regime ($cr$ is not that large).

(iii) The critical radius, when it exists, is at smaller $R$ values for polygons for larger $cr$ values.

(iv) If $L_2 > L_1$ is fixed, then the curve $\nabla C_{cr}(R, L_2)$ has a similar shape to $\nabla C_{cr}(R, L_1)$, but is shifted to the right.

(v) There is an ordered regime for small $R$ values if the crossing number $cr$ is not too large relative to the given length $L_0$.

(vi) Depending on the relationship between the crossing number $cr$ and the length $L_0$, the curves $\nabla C_{cr}(R, L_0)$ have zero, one, or two points of equilibrium.

### *5.5. The different regime in the $(R, L)$ plane.*

To help understand the complex behavior of $\nabla C_{cr}(R, L)$ we present a schema for the $\nabla C_{cr}(R, L)$ surface in the $(R, L)$-plane for a fixed $cr$. Figure 14 shows possible shapes of the depressed, elevated, knotted, and ordered regimes for the same crossing number $cr$. In this plane the line $L = 2R$ separates the confined space from the unconfined space and the unconfined space is a subset of the knotted regime. For completeness we also added the line for $cr = 0$. The critical points form a curve (drawn as a simple line segment) that ends once it hits the unconfined region. In the figure we show three horizontal lines corresponding to to the three curves that are given in Figure 13 and outlined in subsection 5.4 with $cr$ low, medium or high relative to $L_0$. The two vertical lines in Figure 14 correspond to the two curves that are given in Figure 9 and outlined in subsection 5.2 for $cr = 0$ and a $cr > 0$. Finally the slanted line with the label Fig 3 corresponds to the unconfined case shown in Figure 3(a).

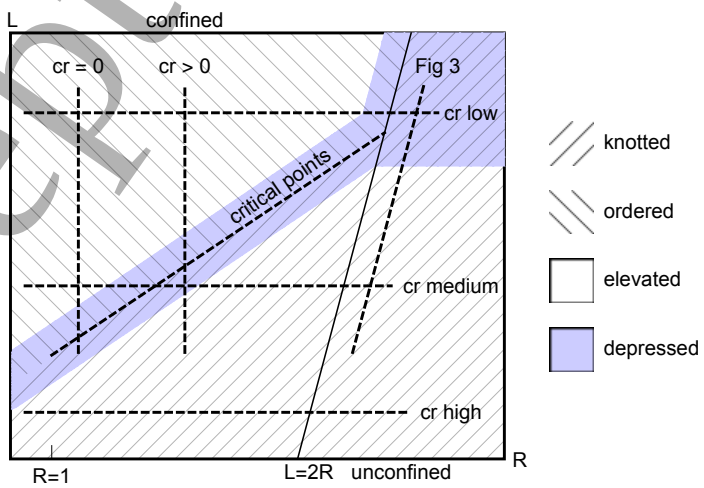


Figure 14: A visualization of the different regimes in the $(R, L)$ plane.

## 6. The effect of knotting complexity on total torsion in the confined case

In this section, we analyze the effects of knotting complexity on the total torsion. The structure of this section is similar to that of the last section on total curvature. In the first part of this section we show graphs from our data and make some observations about the shape of the curves. In the second part of this section we introduce a theoretical model to explain the data in the first part.

As in the case of $C(R, L)$, we normalize $T(R, L)$ by subtracting the average values of the phantom polygons and dividing the result by the length $L$. We denote the resulting quantity by $\nabla T_{cr}(R, L)$.

In looking ahead we note that the behavior of total torsion is often the opposite to the behavior of total curvature. We have already discussed this in Section 3.2 where confinement increases total curvature and decreases total torsion. Similarly, complex knotting under moderate confinement typically requires relatively *more total curvature* than less complex knotting. For total torsion, complex knotting under moderate confinement typically requires relatively *less total torsion* than less complex knotting. However the overall behavior of total torsion is simpler than that of curvature as we did not detect any curves $\nabla T_{cr}(R, L_0)$ or $\nabla T_{cr}(R_0, L)$ with two points of equilibrium. Furthermore there are no critical points and the functions $\nabla T_{cr}(R, L_0)$ or $\nabla T_{cr}(R_0, L)$ are usually monotone decreasing or increasing, respectively. Since the behavior is always in the "knotted" region, we will not use the same language of regimes that we used in the previous section on total curvature.

### *6.1. Numerical results, total torsion, fixed $R_0$*

We first consider $\nabla T_0(R_0, L)$ for a fixed radius $R_0$.

*6.1.1. Numerical results, total torsion, fixed $R_0$, unknotted polygons:* Figure 15 shows typical behaviors of $\nabla T_0(R_0, L)$. The black curve for $R_0 = 3$ from sample 2 is based on $100,000$ polygons. The three dashed curves are from sample 1 for radii surrounding $R_0 = 3$. Comparing the two curves of the same radius $R_0 = 3$ provides an indication of how much the error increases when we use the smaller sample of polygons. We observe:

(i) None of the curves has a point of equilibrium with the phantom polygons. The shape of the curves suggests that an equilibrium value outside the range where we collected data is unlikely. Note that $\nabla T_0(R_0, 5) = 0$, for example, does not count as a true point of equilibrium since there are only unknots when $L < 6$.

(ii) $\nabla T_0(R_0, L)$ appears to be increasing, positive, and concave down for the different values of $R_0$.

(iii) $\nabla T_0(R_0, L)$ appears to approach a horizontal asymptote for large lengths $L$.

(iv) With decreasing radius $R_0$, the curves are shifted up.

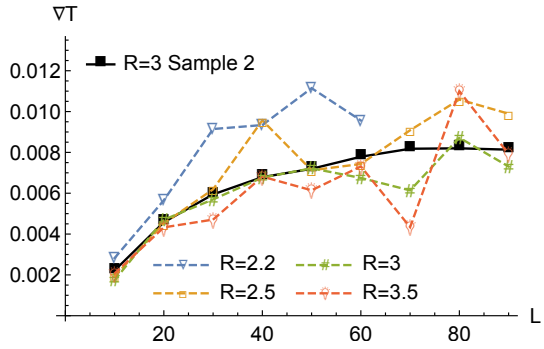


Figure 15: $\nabla T_0(R_0, L)$ for selected values of $R_0$.

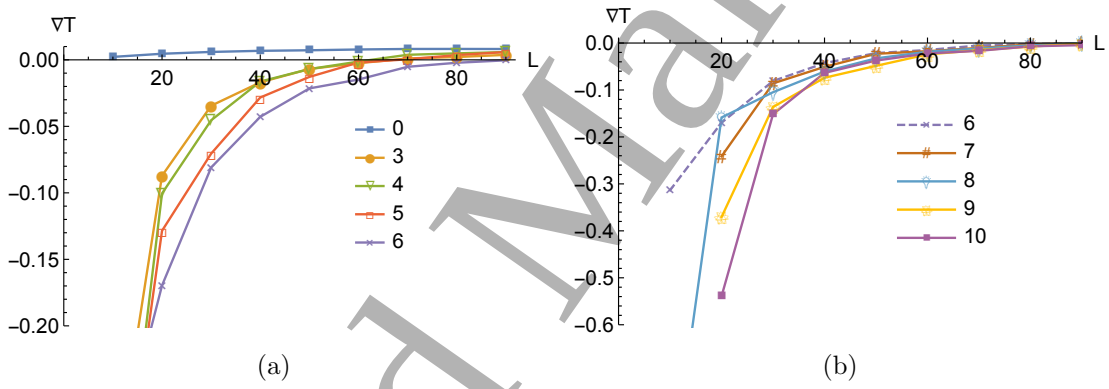


Figure 16: (a) $\nabla T_{cr}(3, L)$ with $cr \leq 6$; (b) $\nabla T_{cr}(3, L)$ with $6 \leq cr \leq 10$.

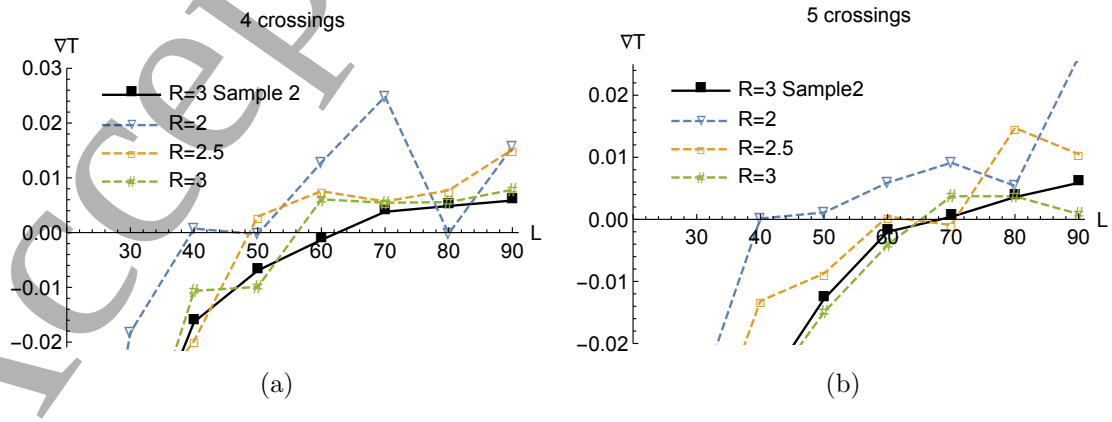


Figure 17: (a) $\nabla T_4(R_0, L)$ for selected values of $R_0$; (b) $\nabla T_5(R_0, L)$ for selected values of $R_0$.

*6.1.2. Numerical results, total torsion, fixed $R_0$, nontrivially knotted polygons separated by crossing number:* Figure 16 shows the numerical plots of $\nabla T_{cr}(3, L)$ for $cr \leq 10$ (the case of $cr = 0$ is included for the purpose of comparison). In addition we show some data of sample 1 in Figure 17 for the curves $\nabla T_4(R_0, L)$ and $\nabla T_5(R_0, L)$ at $R_0 = 2$, $R_0 = 2.5$, and $R_0 = 3$. The data in Figure 17 makes it clear that our observations are not an artifact of the radius $R = 3$. We use the crossing numbers 4 and 5 since it matches the crossing numbers we used in Figure 6. In Figure 17 we use a restricted range for $L$ to enlarge the area around the $L$-axis. We again make several observations:

(i) For $cr = 3, 4, 5$, we see that there are points of equilibrium. It appears that the curves $\nabla T_{cr}(3, L)$ for $cr > 5$ also have a point of equilibrium, but it is outside of our sample range. There is no evidence that there should be a second point of equilibrium for any curve.

(ii) The values of the curves are smallest for short lengths. The graphs are increasing and concave down.

(iii) The curves appear to be approaching a horizontal asymptote. It is not clear if the asymptote is common for all $cr$ values or whether each $cr$ value has its unique asymptotic value.

(iv) The curves $\nabla T_{cr}(3, L)$ are almost perfectly ordered by the reversed order of crossing number, with the unknot curve on top and the 10-crossing curve on the bottom. The differences between the curves are the largest for small $L$ values and they almost disappear for the larger $L$ values.

From Figure 17, we conclude that the points of equilibrium are not an artifact of the radius $R = 3$. In particular, we note that

(i) Decreasing the radius $R$ shifts the equilibrium to the left.

(ii) The curves seem to be ordered by radius, where the smaller radii are on top.

### *6.2. Theoretical model, total torsion, fixed $R_0$*

In this section, we develop a model for the behavior seen in the data above and conjecture on some behavior that lies beyond what we can generate.

*6.2.1. Theoretical model, total torsion, fixed $R_0$, unknotted polygons:* Since all polygons with length fewer than six edges are unknotted [29], we know that $\nabla T_0(R_0, L) = 0$ for $L < 6$. For $L \geq 6$, but close to 6, the average total torsion values of the nontrivial knots are smaller than average for the unknots, and thus we have $\nabla T_0(R_0, L) > 0$ for these $L$ values. As $L$ increases, more and more complicated knots become possible, and these knots have smaller total torsion values, so $\nabla T_0(R_0, L)$ remains positive and increases.

In the last section we made the case that unknotted confined polygons of large lengths seem to require some "ordering" of the edges in the confinement sphere that causes an increase in the average total curvature. This ordered regime leads to an

equilibrium point for total curvature which is not seen without confinement. However, in the case of torsion we found no evidence of a point of equilibrium and no evidence of a reversal of the ordering of the curves.

Furthermore all curves seem to settle on a horizontal asymptote. Thus we propose that this "ordering" of the edges has no effect on the total torsion of the unknotted random polygons. We could speculate that all curves settle $\nabla T_0(R_0, L)$ on a common horizontal asymptote that is above the $L$-axis. However our data with $L \leq 90$ provides insufficient evidence to support this conjecture.

*6.2.2. Theoretical model, total torsion, fixed $R_0$, nontrivially knotted polygons separated by crossing number:* This case is similar to the previous case except that $\nabla T_{cr}(R_0, L) < 0$ for small $L$ since most short chains are unknotted. As $L$ increases, the polygons with a fixed crossing number $cr$ eventually have a lower topological complexity than the phantom polygons and thus $\nabla T_{cr}(R_0, L)$ crosses the $L$-axis and becomes positive. Thus there exists a point of equilibrium. Decreasing the radius moves this point of equilibrium to the left. Unlike the case for total curvature, there is no evidence of a second point of equilibrium. All functions are concave down and seem to settle on a positive horizontal asymptote as $L$ increases. Note that since we define $\nabla T_{cr}$ as the torsion difference per edge, this means that the total torsion difference between knots of a fixed crossing number and the phantom polygons increases linearly with length, which agrees with the observations made in the unconfined case [28].

Sketches of the graphs arising for $cr = 0$ and $cr > 0$ are shown in Figure 18. For $cr > 0$, we show two curves with two different crossing numbers $cr_2 > cr_1$.

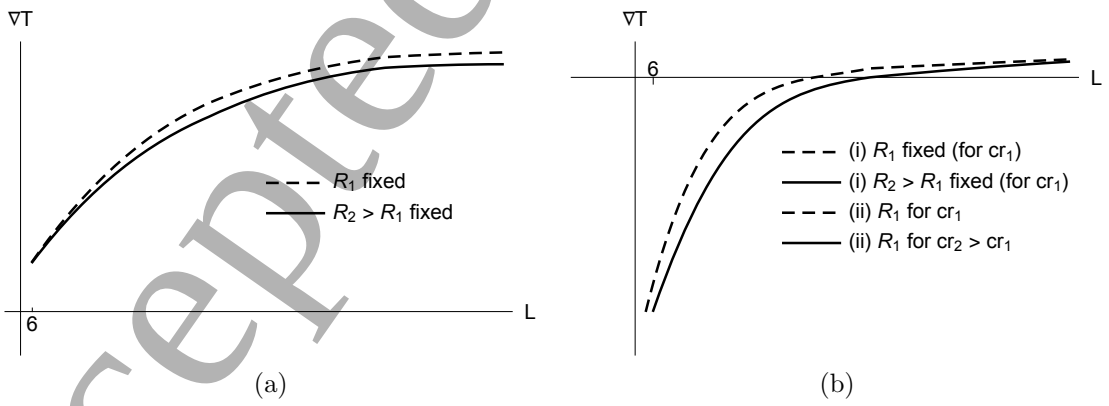


Figure 18: (a) $\nabla T_0(R_0, L)$ for two different values of $R_0$, $R_2 > R_1$; (b) $\nabla T_{cr}(R_0, L)$ for two different values of $R_0$, $R_2 > R_1$, and two crossing numbers, $cr_2 > cr_1$. The two different interpretations of the curves are indicated by (i) and (ii).

*6.3. Numerical results, total torsion, fixed $L_0$*

Next we consider $\nabla T_0(R, L_0)$ for a fixed length $L_0$.

*6.3.1. Numerical results, total torsion, fixed $L_0$, unknotted polygons:* Figure 19 shows examples of the typical behaviors of $\nabla T_0(R, L_0)$. The black curve for $L_0 = 30$ from sample 2 is based on 100,000 polygons. The three dashed curves are from sample 1 for radii and lengths surrounding $L_0 = 30$. Comparing the two curves of the same length $L_0 = 30$ provides some indication of how much the error increases when we use the smaller sample of polygons. We observe:

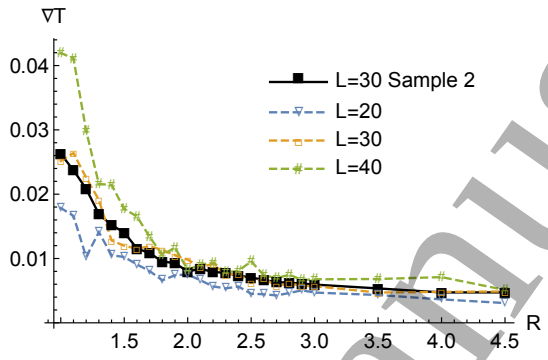


Figure 19: $\nabla T_0(R, L_0)$ for selected values of $L_0$.

(i) None of the curves has a point of equilibrium with the phantom polygons. The shape of the curves suggests that an equilibrium value outside the range where we collected data is unlikely.

(ii) $\nabla T_0(R, L_0)$ is strictly decreasing and positive for the different values of $L_0$.

(iii) The curves $\nabla T_0(R, L_0)$ appear to approach a horizontal asymptote as $R \to \infty$.

(iv) With increasing length $L_0$, the curves are shifted up.

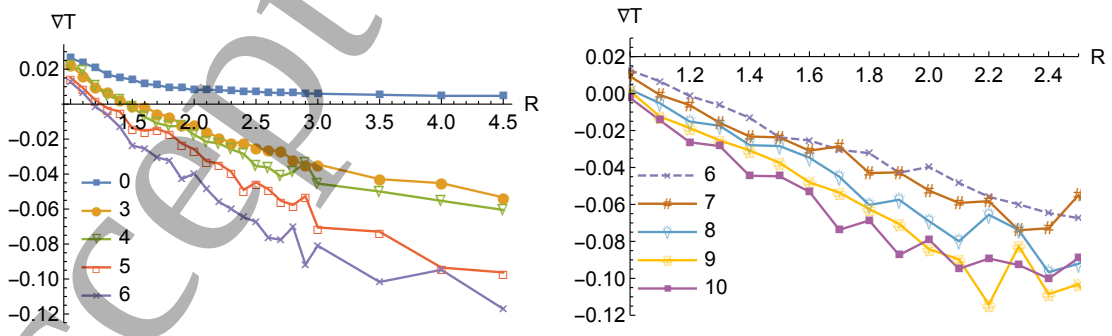


Figure 20: (a) $\nabla T_{cr}(R, 30)$ with $cr \leq 6$; (b) $\nabla T_{cr}(R, 30)$ with $6 \leq cr \leq 10$ and $1 \leq R \leq 2.5$.

*6.3.2. Numerical results, total torsion, fixed $L_0$, nontrivially knotted polygons separated by crossing number:* Figure 20 shows the numerical plots of $\nabla T_{cr}(R, 30)$ for $cr \leq 10$.

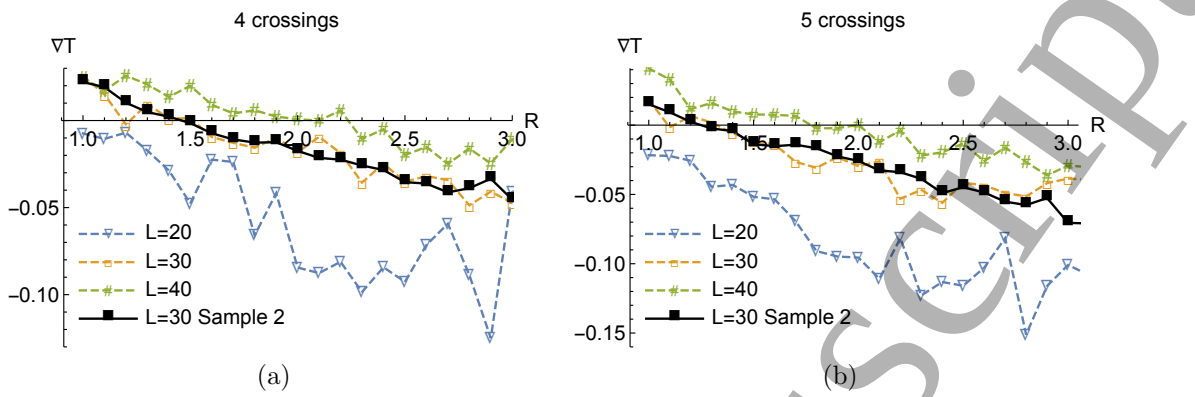


(a) (b)

Figure 21: (a) $\nabla T_4(R, L_0)$ for selected values of $L_0$; (b) $\nabla T_5(R, L_0)$ for selected values of $L_0$.

For the larger crossing numbers (Figure 20(b)) we show only the range of radii $1 \leq R \leq 2.5$ since knots of complexity $cr \geq 7$ are rare at $R > 2.5$. In addition, we show some data from sample 1 in Figure 21, for $cr = 4$ and $cr = 5$ similar to what we showed in Figure 17. As before, the data in Figure 21 makes it clear that our observations are not an artifact of the length $L_0 = 30$. In Figure 21 we use a restricted range of $R$ to enlarge the area around the $R$-axis. We observe:

(i) There appears to be one point of equilibrium for each $cr \geq 3$. There is no evidence that there should be a second point of equilibrium for any curve. For $cr \leq 8$, the curves are positive at $R = 1$ and the existence of an equilibrium is clear. One would assume that for the $cr$ values of 9 and 10 the curves would be positive at an $R$ value slightly less than one. In particular, one might conjecture that for each $cr$ and $L_0$, there is an $R_0$ such that $\nabla T_{cr}(R_0, L_0) > 0$. Also, each of the curves decreases for $R > 1$, nearly linearly, but slightly concave upward.

(ii) The curves do not appear to be approaching a horizontal asymptote within the range of our data.

(iii) The curves $\nabla T_{cr}(R, 30)$ are almost perfectly ordered by the reversed order of crossing number, with the unknot on top and the 10-crossing curve on the bottom. The differences between the curves are the smallest for small $R$ values and get larger as $R$ increases.

From Figure 21 we conclude that the points of equilibrium are not an artifact of the length $L = 30$. In particular,

(i) Increasing the length $L$ shifts the points of equilibrium to the left.

(ii) The curves are ordered by lengths, with the larger lengths on top.

### *6.4. Theoretical model, total torsion, fixed $L_0$*

We now want to consider the situation where the length $L_0$ is fixed and the radius varies. As one guiding principle we use the idea that keeping the confinement radius fixed and increasing the length is in some sense analogous to keep the length fixed and decreasing the confinement radius.

We believe there are three possible behaviors (*cr* small, medium, or large when compared to the fixed length $L_0$) just like in the case of total curvature. We note that the case *cr* "small" is observed for $cr = 0$, and the case *cr* "medium" is also observed in our data. However the case *cr* "large" is not observed within the range of our data, and is therefore purely conjecture.

As before, we describe the behavior for decreasing $R$ values, i.e. increasing confinement pressure. We begin with the two extreme cases (small and large *cr* values relative to $L_0$) and then tackle the *cr* medium behavior.

*6.4.1. Theoretical model, total torsion, fixed $L_0$, cr is small:* For $R > L_0/2$, there is no confinement pressure. Since *cr* is small relative to $L_0$, the phantom polygons are much more complicated on average than the *cr*-crossing knot type configurations. Thus, the *cr*-crossing knots have higher total torsion values on average than the phantom polygons and we have $\nabla T_{cr}(R, L_0) > 0$ for $R \geq L_0/2$.

As $R$ decreases below $L_0/2$, confinement pressure increases, which results in more complicated knotting, on average. This more complicated knotting has smaller average total torsion values than the *cr*-crossing polygons, which then lowers the phantom polygon average relative to the *cr*-crossing average. There is no evidence that the edge organization (leading to the ordered regime for total curvature) has any effect on the average total torsion. Thus, the value $\nabla T_{cr}(R, L_0)$ increases as $R$ decreases from $L_0/2$ to one. Although we have no information from our computations for $R < 1$, we conjecture that $\nabla T_0(R, L_0) > 0$ for all $R \geq 1/2$, see Figure 22(a).

If $L_1 > L_2 \geq 6$ and *cr* is small for both $L_1$ and $L_2$, we expect $\nabla T_{cr}(R, L_1) > \nabla T_{cr}(R, L_2)$ for all $R$ since the average complexity of knots at length $L_1$ is higher than the average complexity of knots at length $L_2$, see Figure 22(a).

*6.4.2. Theoretical model, total torsion, fixed $L_0$, cr is high:* Suppose $L_0$ is such that *cr*-crossing knots can barely be created with $L_0$ edges (even under confinement). In this case, regardless of $R$, we expect *cr*-crossing knots to be more complicated on average than the phantom polygons. Thus, we expect $\nabla T_{cr}(R, L_0) < 0$ for all values of $R$ when *cr* is high. As $R$ decreases, more complicated knot types comprise a higher percentage of the phantom polygons, which decreases the difference between the average total torsion over *cr*-crossing knots and the phantom polygons. So we expect $\nabla T_{cr}(R, L_0)$ to rise to values closer to 0 as $R$ decreases, see Figure 22(c).

*6.4.3. Theoretical model, total torsion, fixed $L_0$, cr is medium:* This situation is what we observe for $3 \leq cr \leq 10$ in the graphs. For $R \geq L_0/2$, the value of $\nabla T_{cr}(R, L_0)$ is constant, and negative since $cr$-crossing knots are more complicated than knots which comprise most of the phantom polygons. As $R$ decreases, the confinement pressure increases the average complexity of the knots in the phantom polygon population. As such, the values of $\nabla T_{cr}(R, L_0)$ approach 0. As $R$ continues to decrease, knots even more complicated than the $cr$-crossing knots begin to dominate the phantom polygons, and these have lower average total torsion values than the $cr$-crossing knots. So $\nabla T_{cr}(R, L_0)$ achieves an equilibrium and increases as $R$ decreases. Note that we observe this full behavior for $3 \leq cr \leq 8$. It seems clear that $cr = 9, 10$ are following the same behavior, but the equilibrium value is somewhere between 1/2 and 1. It is unclear what happens when $1/2 \leq R \leq 1$, see Figure 22(b).

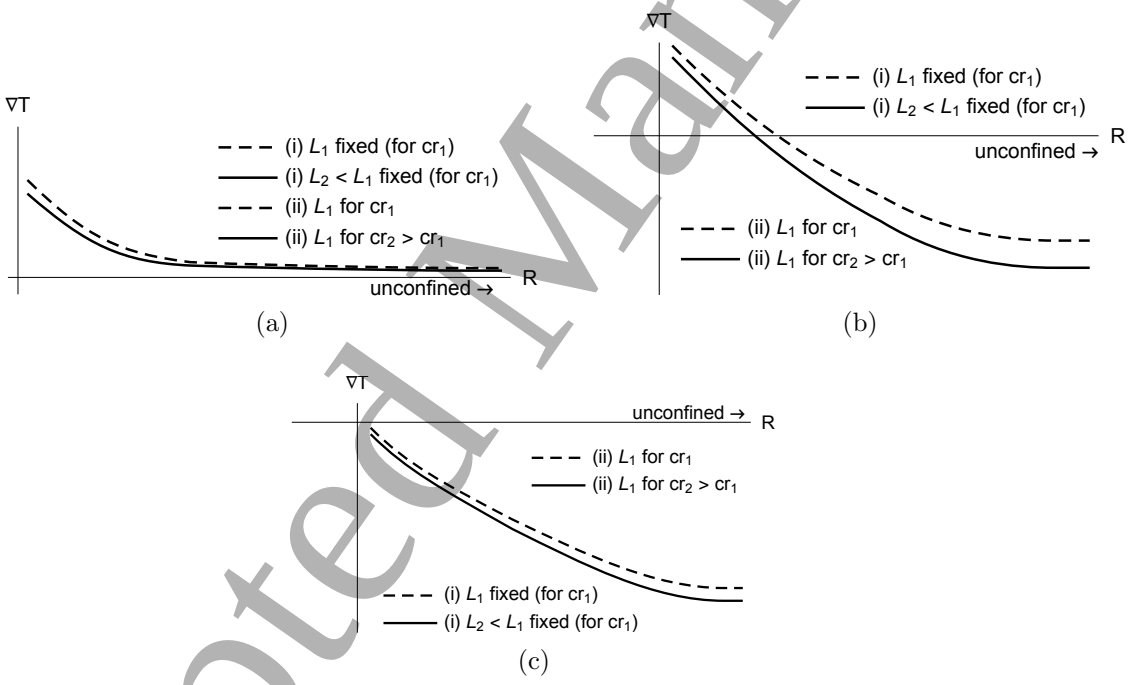


Figure 22: (a) $\nabla T_{cr}(R, L_0)$ for $cr$ small, $cr_2 > cr_1$, and two different lengths $L_0$, $L_2 < L_1$; (b) $\nabla T_{cr}(R, L_0)$ for $cr$ medium, $cr_2 > cr_1$, and two different lengths $L_0$, $L_2 < L_1$; (c) $\nabla T_{cr}(R, L_0)$ for $cr$ large, $cr_2 > cr_1$, and two different lengths $L_0$, $L_2 < L_1$.

## 7. The effect of prime versus composite and of alternating versus non-alternating.

In this section, we explore how some special knot families affect the total curvature and total torsion of random polygons under confinement. In particular, we compare the alternating knot types with the non-alternating ones, and we compare prime knot types with composite knot types.

There exist several knot energy functionals (such as ropelength [3, 7, 20, 24, 26] or Möbius energy [17, 25]) that have larger values for alternating knots than for non-alternating knots of the same crossing numbers. In fact, in the world of physical knot theory alternating knots are considered to be more complicated than non-alternating knots with the same crossing number. We see this effect for confined polygons as well.

### *7.1. Effect of alternating vs non-alternating knot types*

In this subsection we compare the average total curvature and average total torsion between alternating and non-alternating knot types with the same crossing number. One might expect that random polygons representing alternating prime knots have overall higher total curvatures and lower total torsions than those of random polygons representing non-alternating prime knots of the same crossing number. Our numerical study, in fact, supports this expectation. We show data for 8-, 9- and 10-crossing knot types, that is normalized by taking the curvature (or torsion) per turn for the alternating prime knots with $cr$ crossings minus the curvature (or torsion) per turn for the non-alternating prime knots with $cr$ crossings and denoted by $C_\Delta$ (or $T_\Delta$), see Figures 23 and 24. In Figure 23(a) we show $C_\Delta$ versus length $L$ and in Figure 23(b) we show $C_\Delta$ versus radius $R$. Notice that we only show this data for radii $R \leq 2.5$. For radii $R > 2.5$ there are few knots of this complexity and the data is not reliable, fluctuating widely. A similar fluctuation can be observed for $L \leq 30$ in Figure 23(a).

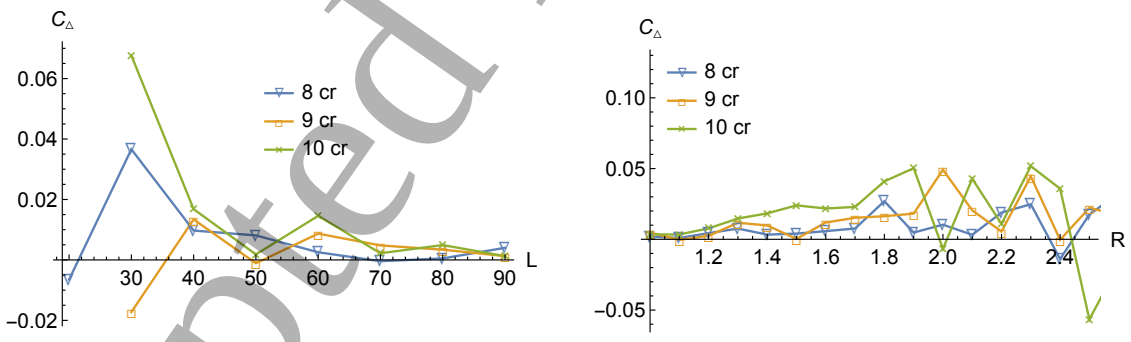


(a) (b)

Figure 23: The difference in curvature $C_\Delta$ (per edge) of knotted random polygons that are of alternating prime knot types minus knotted random polygons that are of non-alternating prime knot types versus (a) length with $R_0 = 3$ and (b) radius with $L_0 = 30$.

In Figure 24(a) we show $T_\Delta$ versus length $L$ and in Figure 24 (b) we show $T_\Delta$ versus radius $R$. Note that we only show this data for radii $R \leq 2.5$ for the same reasons as before.

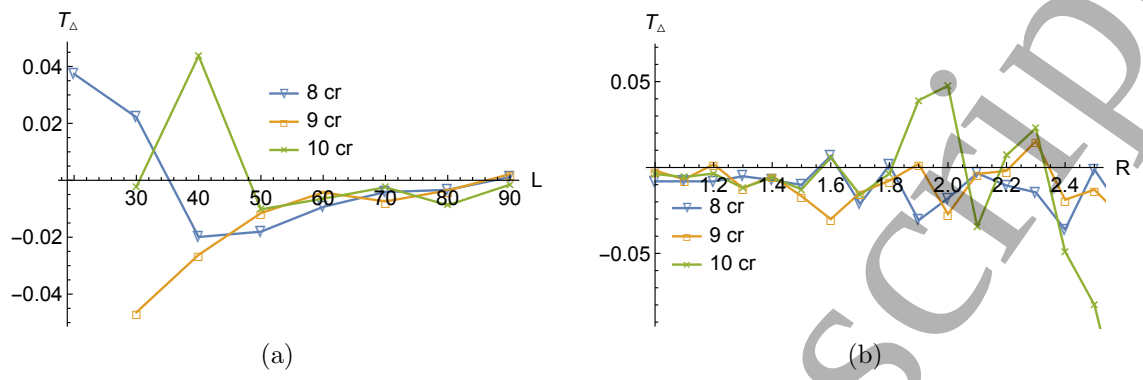


(a) (b)

Figure 24: The difference in torsion $T_\Delta$ (per edge) of knotted random polygons that are of alternating prime knot types minus knotted random polygons that are of non-alternating prime knot types versus (a) length with $R_0 = 3$ and (b) radius with $L_0 = 30$.

### *7.2. Effect of prime versus composite knot types*

In this subsection we compare composite knot types with prime knot types of the same crossing number. For polygons with the same crossing number and length, our data suggests that the composite knot types have larger total curvature and smaller total torsion than the prime knot types. Figures 25 and 26 show the difference between the curvature per edge of the composite knot $3_1\#3_1$ (or $3_1\#4_1$) minus the curvature per edge of the 6- (or 7-) crossing prime knots. We see that the curvature of the composite knots is larger than the curvature of the prime knots of the same crossing number. In the case of 6-crossing knots, the case is pretty convincing. In the case of 7-crossing knots, the evidence is not as convincing. However, we need to keep in mind that we have fewer knots for the shorter lengths and thus larger error margins. We also see that there is no apparent pattern to the differences between the different prime knots.

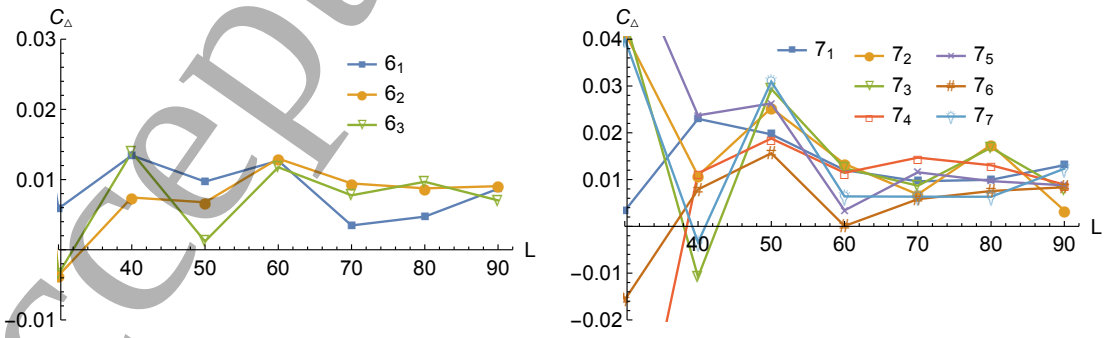


(a) (b)

Figure 25: (a) The curvature difference (per edge) between random polygons that are prime knots with (a) 6-crossings and (b) 7-crossings and composite knot types with the same number of crossings. All polygons are for radius $R_0 = 3$ and arise from sample 2.

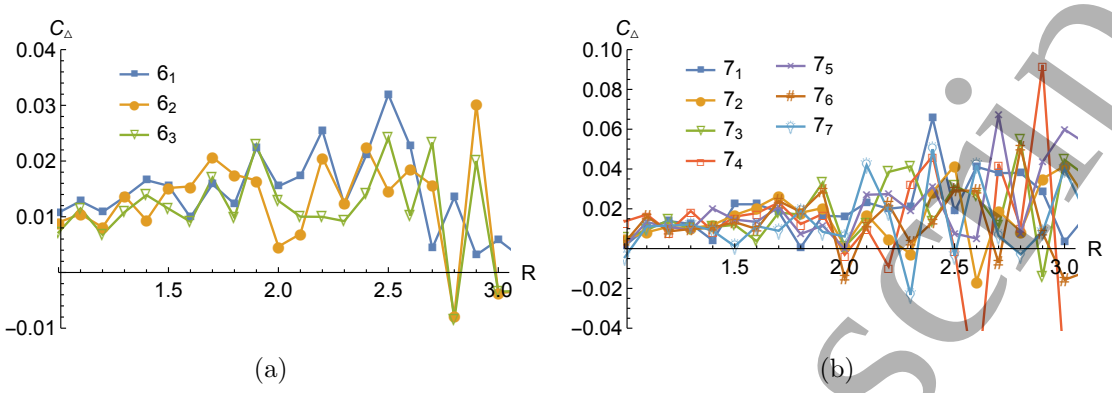


Figure 26: (a) The curvature difference (per edge) between random polygons that are prime knots with (a) 6-crossings and (b) 7-crossings and composite knot types with the same number of crossings. All polygons are for length $L_0 = 30$ and arise from sample 2.

Figures 27 and 28 show the difference between the torsion per edge of the composite knot $3_1\#3_1$ (or $3_1\#4_1$) minus the torsion per edge of the 6- (or 7-) crossing prime knots. We can see that the torsion of the composite knots is smaller than the torsion of the prime knots of the same crossing number. Similar to the case of the curvature, the evidence for 6-crossing knots is quite convincing that the prime knots have higher total torsions than the composite knot but the evidence for 7-crossing knots is not as convincing.

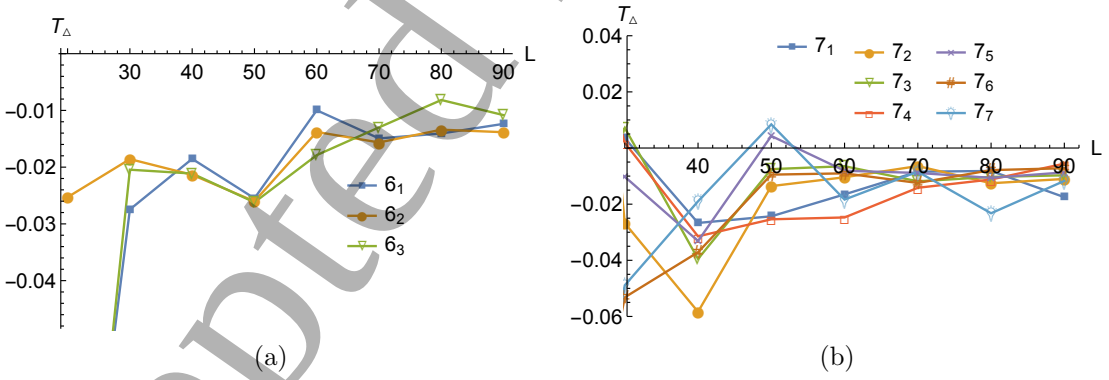


Figure 27: (a) The torsion difference (per edge) between random polygons that are prime knots with (a) 6-crossings and (b) 7-crossings and composite knot types with the same number of crossings. All polygons are for radius $R_0 = 3$ and arise from sample 2.

## 8. Conclusions

In this paper, we have discussed the effects on total curvature and total torsion of changing the length of random confined polygons while keeping confinement constant and of changing the radius of confinement of random confined polygons while keeping the

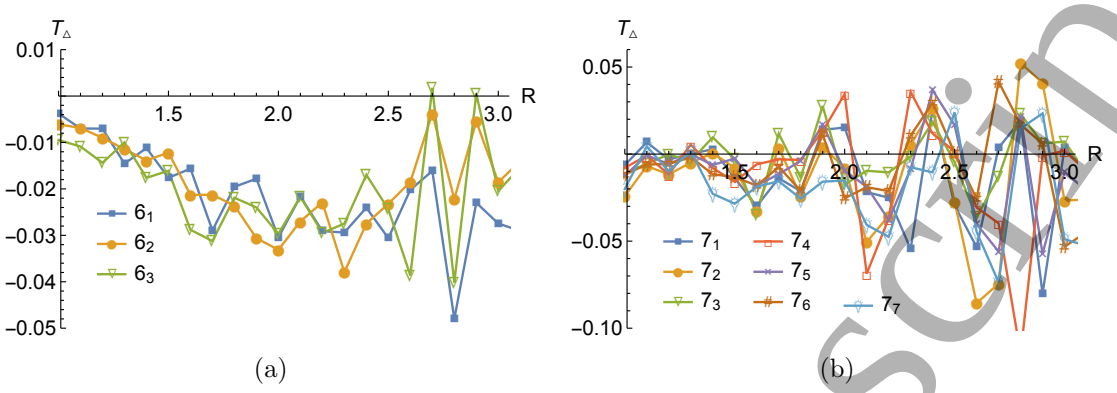


(a) (b)

Figure 28: (a) The torsion difference (per edge) between random polygons that are prime knots with (a) 6-crossings and (b) 7-crossings and composite knot types with the same number of crossings. All polygons are for length $L_0 = 30$ and arise from sample 2.

length constant. In particular we study these effects for polygons of a fixed topological complexity. We summarize our results below.

*Effect on total curvature*: It has been observed that knotting complexity increases total curvature in the case of unconfined polygons for all lengths. This is no longer true once we have confined polygons. In some instances confinement changes the ordering and topologically less complex polygons can have a larger total curvature than topologically more complex polygons. In general, the effect of confinement on total curvature is much stronger than the effect of knotting complexity. Strong confinement increases total curvature drastically. In order to detect the effects of topological complexity we study the difference in total curvature between the phantom polygons and polygons of a fixed topological complexity. Under very strong confinement, configurations from simpler knot types appear to require some organization to the edges which increases the average total curvature relative to the phantom polygons. This edge organization changes the behavior of equilibrium values. In particular, we find that additional points of equilibrium were created under confinement. In the unconfined case, there is no point of equilibrium for the unknot. Under confinement, the unknot has one point of equilibrium. In the unconfined case, there is (typically) one point of equilibrium for each $cr \geq 3$. Under confinement, we (typically) have two points of equilibrium. We also find that alternating knots often have a slightly higher total curvature than non-alternating knots of the same crossing number. Likewise, the total curvature of the composite knots is often slightly larger than the total curvature of the prime knots with the same crossing number.

*Effect on total torsion*: It has been observed that knotting complexity decreases total torsion in the case of unconfined polygons for all lengths. This is also true for confined random polygons. In general, the effect of confinement on total torsion is much stronger than the effect of knotting complexity. Strong confinement decreases total torsion drastically. In order to detect the effects of topological complexity we

studied the difference in total torsion between the phantom polygons and polygons of a fixed topological complexity. The edge organization which boosts the average total curvature of simple knots under very strong confinement does not appear to affect the average total torsion. Thus, the number of equilibrium values is the same for unconfined and confined polygons. In both the confined and the unconfined case, there is no point of equilibrium for the unknot and one point of equilibrium for each $cr \geq 3$. We also find that alternating knots often have a slightly lower total torsion than non-alternating knots of the same crossing number, and that the total torsion of the composite knots is often slightly smaller than the total torsion of the prime knots of the same crossing number.

*Total curvature versus total torsion:* The effect on total torsion and total curvature are often the opposite: Confinement increases total curvature and decreases total torsion, often knotting increases total curvature and decreases total torsion. When the curves in our graphs are increasing for total curvature, they are decreasing for total torsion. When the curves are concave up for total curvature, then they are concave down for total torsion. In the presentations of our numerical results, we did not include any error bars. In many cases the error bars are larger than the space that separates two adjacent curves. However, our data is convincing when one considers the consistency in the patterns exhibited in our numerical results.

*Additional Remarks:*

(i) The differences between a random polygon and a random walk in confinement are not as strong as without confinement because the distance between the two ends of the random walk is bounded by the diameter of the confinement sphere. Provided that one has a reasonable definition of knotting in a polygonal walk, one would expect that the results of this study carry over directly to random confined walks in strong confinement.

(ii) The points of equilibrium between torsion and curvature do not coincide. In [15], a geometric quantity called the average crossing number was studied. It behaves similar to torsion in the sense that non-trivially knotted polygons of a fixed crossing number have a single point of equilibrium with the phantom polygons. While there is some similarity between the location of the points of equilibrium for torsion and for the average crossing number versus both the confinement radius and length, none of the equilibria coincide with each other. Similarly, in [30], the authors found that different geometric values yielded different equilibrium values in the unconfined case. Thus, it seems that different geometric measurements have different points of equilibrium.

(iii) In [8] we recorded under what conditions (given a fix length and confinement radius) the probability to obtain knots with a fixed crossing number reaches its maximum. Thus if one wanted to sample random polygonal knots with a fixed crossing number then one could chose optimal conditions to yield these polygons with a fixed topological crossing number. However these maxima do not correlate well with the equilibrium of the various geometric quantities.

(iv) One could ask the question how do the equations (3) and (4) for $C(R, L)$ and $T(R, L)$ change if one restricts the sample to random polygons of a fixed topological complexity. We do not have a good model for this, because our sample size is not large enough. This is particular apparent in two cases: complex knots ($cr \geq 8$) and short length ($L \leq 20$) or simple knots ($cr \leq 6$) and long length ($L \geq 60$). In these areas the noise level of our data increases significantly due to the lower probability of knots types of these complexities. Figure 29 shows the result of fitting total curvature and total torsion data for 5-crossing knots with the given equations. The figure indicates that the total curvature and total torsion might follow the given equations but without more data this cannot be said with any certainty. In addition, we want to point out that the values of $a$ and $b$ are slightly different when compared to the phantom polygons in Figure 2(c) and thus the best fit curves for the phantom polygons and the 5 crossing knots will move apart with increasing length $L$.

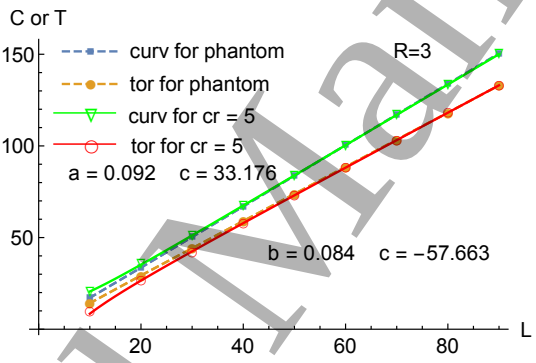


Figure 29: Using equations (3) and (4) to fit total curvature and total torsion data for 5-crossing knots. The given a and c values are for the 5-crossing data, the ones from the phantom are shown in Figure 2 (c). The R-squared values for the fit are 0.99999 and 0.99998 for curvature and torsion, respectively. The phantom data is given as a dashed line.

(v) As a final remark we want to point out that our study included other geometric measures, such as the average crossing number and the writhe, and we will report on our findings in a future paper [15]. Also it would be interesting to study the effects on total curvature and total torsion of random polygons in strong confinement with confinement radii $R < 1$. However, we currently have no means to generate such polygons with uniform probability.

[1] Jorge Alberto Calvo. Geometric knot spaces and polygonal isotopy. *J. Knot Theory Ramifications*, 10(2):245–267, 2001. Knots in Hellas '98, Vol. 2 (Delphi).

[2] Jason Cantarella, Tetsuo Deguchi, and Clayton Shonkwiler. Probability theory of random polygons from the quaternionic viewpoint. *Communications on Pure and Applied Mathematics*, 67(10):1658–1699, 2014.

[3] Jason Cantarella, Robert B. Kusner, and John M. Sullivan. On the minimum ropelength of knots and links. *Invent. Math.*, 150(2):257–286, 2002.

[4] Jason Cantarella and Clayton Shonkwiler. The symplectic geometry of closed equilateral random walks in 3-space. *Ann. Appl. Probab.*, 26(1):549–596, 2016.

[5] Lucia Coronel, Enzo Orlandini, and Cristian Micheletti. Non-monotonic knotting probability and knot length of semiflexible rings: the competing roles of entropy and bending energy. *Soft Matter*, 13:4260–4267, 2017.

[6] Yuanan Diao. The knotting of equilateral polygons in $\mathbf{R}^3$. *J. Knot Theory Ramifications*, 4(2):189–196, 1995.

[7] Yuanan Diao, Claus Ernst, and E. J. Janse van Rensburg. Knot energies by ropes. *J. Knot Theory Ramifications*, 6(6):799–807, 1997.

[8] Yuanan Diao, Claus Ernst, Anthony Montemayor, Eric Rawdon, and Uta Ziegler. The knot spectrum of confined random equilateral polygons. *Molecular Based Mathematical Biology*, 2(1):19–33, 2014.

[9] Yuanan Diao, Claus Ernst, Anthony Montemayor, and Uta Ziegler. Generating equilateral random polygons in confinement. *J. Phys. A: Math. Theor*, 44:405202, 2011.

[10] Yuanan Diao, Claus Ernst, Anthony Montemayor, and Uta Ziegler. Generating equilateral random polygons in confinement II. *J. Phys. A: Math. Theor*, 45:275203, 2012.

[11] Yuanan Diao, Claus Ernst, Anthony Montemayor, and Uta Ziegler. Generating equilateral random polygons in confinement III. *J. Phys. A: Math. Theor*, 45:465003, 2012.

[12] Yuanan Diao, Claus Ernst, Anthony Montemayor, and Uta Ziegler. Curvature of random walks and random polygons in confinement. *J. Phys. A: Math. Theor.*, 46(28):285201, 2013.

[13] Yuanan Diao, Claus Ernst, Eric J. Rawdon, and Uta Ziegler. Relative frequencies of alternating and nonalternating prime knots and composite knots in random knot spaces. *Experimental Mathematics*, 0(0):Experimental Mathematics, 2017. https://doi.org/10.1080/10586458.2017.1320239.

[14] Yuanan Diao, Claus Ernst, and Uta Ziegler. Random walks and polygons in tight confinement. *Journal of Physics: Conference Series*, 544(1):012017, 2014.

[15] Yuanan Diao, Claus Ernst, Uta Ziegler, and Eric J. Rawdon. Average crossing number and writhe of knotted random polygons in confinement. preprint, 2018.

[16] Yuanan Diao, Claus Ernst, Uta Ziegler, and Eric J. Rawdon. The knot spectrum of random knot spaces. In Philipp Reiter, Simon Blatt, and Armin Schikorra, editors, *New Directions in Geometric and Applied Knot Theory*. De Gruyter, Berlin, 2018.

[17] Michael H. Freedman, Zheng-Xu He, and Zhenghan Wang. Möbius energy of knots and unknots. *Ann. of Math. (2)*, 139(1):1–50, 1994.

[18] P. Freyd, D. Yetter, J. Hoste, W. B. R. Lickorish, K. Millett, and A. Ocneanu. A new polynomial invariant of knots and links. *Bull. Amer. Math. Soc. (N.S.)*, 12(2):239–246, 1985.

[19] Eric Furstenberg, Jie Li, and Jodi Schneider. Stick knots. *Chaos Solitons Fractals*, 9(4-5):561–568, 1998. Knot theory and its applications.

[20] Oscar Gonzalez and John H. Maddocks. Global curvature, thickness, and the ideal shapes of knots. *Proc. Natl. Acad. Sci. USA*, 96(9):4769–4773, 1999.

[21] Alexander Y. Grosberg. Total curvature and total torsion of a freely jointed circular polymer with $n >> 1$ segments. *Macromolecules*, 41(12):4524–4527, 2008.

[22] Jim Hoste and Morwen Thistlethwaite. Knotscape. http://www.math.utk.edu/ morwen/knotscape.html. Program for computing topological information about knots.

[23] Youngsik Huh and Seungsang Oh. An upper bound on stick number of knots. *Journal of Knot Theory and Its Ramifications*, 20(05):741–747, 2011.

[24] Vsevolod Katritch, Jan Bednar, Didier Michoud, Robert G. Scharein, Jacques Dubochet, and Andrzej Stasiak. Geometry and physics of knots. *Nature*, 384:142–145, 1996.

[25] Robert B. Kusner and John M. Sullivan. Möbius energies for knots and links, surfaces and submanifolds. In *Geometric topology (Athens, GA, 1993)*, pages 570–604. Amer. Math. Soc., Providence, RI, 1997.

[26] Richard A. Litherland, Jonathan Simon, Oguz Durumeric, and Eric Rawdon. Thickness of knots.

*Topology Appl.*, 91(3):233–244, 1999.

[27] Seiya Negami. Ramsey theorems for knots, links and spatial graphs. *Trans. Amer. Math. Soc.*, 324(2):527–541, 1991.

[28] Patrick Plunkett, Michael Piatek, Akos Dobay, John C. Kern, Kenneth C. Millett Millett, Andrzej Stasiak, and Eric J. Rawdon. Total curvature and total torsion of knotted polymers. *Macromolecules*, 40(10):3860–3867, 2007.

[29] Richard Randell. An elementary invariant of knots. *J. Knot Theory Ramifications*, 3(3):279–286, 1994. Random knotting and linking (Vancouver, BC, 1993).

[30] Eric Rawdon, Akos Dobay, John C. Kern, Kenneth C. Millett, Michael Piatek, Patrick Plunkett, and Andrzej Stasiak. Scaling behavior and equilibrium lengths of knotted polymers. *Macromolecules*, 41(12):4444–4451, 2008.

[31] Eric J. Rawdon and Robert G. Scharein. Upper bounds for equilateral stick numbers. In *Physical knots: knotting, linking, and folding geometric objects in* $\mathbb{R}^3$ *(Las Vegas, NV, 2001)*, volume 304 of *Contemp. Math.*, pages 55–75. Amer. Math. Soc., Providence, RI, 2002.